Inorganic Chemistry

Article

pubs.acs.org/IC

Ferric Heme-Nitrosyl Complexes: Kinetically Robust or Unstable Intermediates?

Ashley B. McQuarters,[†] Jeff W. Kampf,[†] E. Ercan Alp,[‡] Michael Hu,[‡] Jiyong Zhao,[‡] and Nicolai Lehnert*[,†]

[†]Department of Chemistry and Department of Biophysics, University of Michigan, Ann Arbor, Michigan 48109, United States

[‡]Advanced Photon Source, Argonne National Laboratory, Argonne, Illinois 60439, United States

Supporting Information

ABSTRACT: We have determined a convenient method for the bulk synthesis of high-purity ferric heme-nitrosyl complexes ({FeNO}^{6} in the Enemark–Feltham notation); this method is based on the chemical or electrochemical oxidation of corresponding {FeNO}^{7} precursors. We used this method to obtain the five- and six-coordinate complexes [Fe(TPP)(NO)]$^+$ (TPP^{2-} = tetraphenylporphyrin dianion) and [Fe(TPP)(NO)(MI)]$^+$ (MI = 1-methylimidazole) and demonstrate that these complexes are stable in solution in the absence of excess NO gas. This is in stark contrast to the often-cited instability of such {FeNO}^{6} model complexes in the literature, which is likely due to the common presence of halide impurities (although other impurities could certainly also play a role). This is avoided in our approach for the synthesis of {FeNO}^{6} complexes via oxidation of pure {FeNO}^{7} precursors. On the basis of these results, {FeNO}^{6} complexes in proteins do not show an increased stability toward NO loss compared to model complexes. We also prepared the halide-coordinated complexes [Fe(TPP)(NO)(X)] (X = Cl$^-$, Br$^-$), which correspond to the elusive, key reactive intermediate in the so-called autoreduction reaction, which is frequently used to prepare {FeNO}^{7} complexes from ferric precursors. All of the complexes were characterized using X-ray crystallography, UV–vis, IR, and nuclear resonance vibrational spectroscopy (NRVS). On the basis of the vibrational data, further insight into the electronic structure of these {FeNO}^{6} complexes, in particular with respect to the role of the axial ligand *trans* to NO, is obtained.

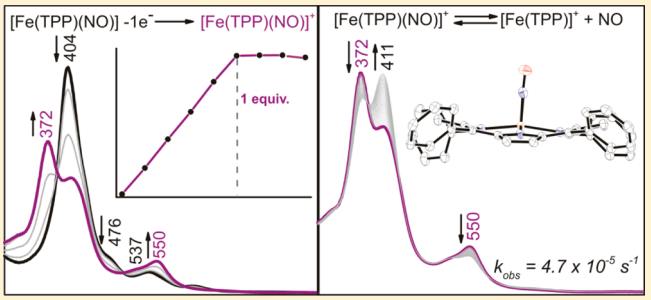

INTRODUCTION

Nitric oxide (NO) is a toxic gas that has surprisingly important roles in biological systems. In mammals, NO plays a crucial role in nerve-signal transduction, vasodilation, and immune response by white blood cells.[1−3] NO is produced in vivo by the nitric oxide synthase (NOS) family of enzymes.[4,5] In mammals, NO produced by endothelial NOS in the cardiovascular system is sensed by and subsequently activates soluble guanylate cyclase (sGC), and in this way, it modulates arterial vasodilation.[6] Interestingly, certain blood-sucking insects such as *Rhodnius proxlixus* (known as the "kissing bug") and *Cimex lectularius* (known as the "bed bug") take advantage of NO's vasodilating effect. When these insects bite a victim, they use small NO-carrier proteins called nitrophorins (Nps) to inject NO into the bite to increase their blood meal.[7] Nps use ferric heme-nitrosyl complexes, or {FeNO}^{6} in the Enemark–Feltham notation (where the superscript 6 represents the number of iron d electrons plus the unpaired electrons in the π^* orbitals of NO),[8] for NO transport. Ferric heme-nitrosyl complexes are also important intermediates in dissimilatory denitrification.[9−11] Heme {FeNO}^{6} complexes in proteins are generally six-coordinate (6C) and contain either a neutral N-donor ligand such as histidine (His) or an anionic S-donor ligand such as cysteinate (Cys) as a *trans* ligand to NO. Due to the significance of ferric heme-nitrosyl complexes in biology, it is important to understand their basic properties and reactivity. Synthetic model complexes are a great tool to study the fundamental properties of these complexes and in comparison to the proteins, identify the different roles that the protein matrix plays in modulating their geometric and electronic structures, properties, and reactivities. In the case of {FeNO}^{6} complexes, proteins usually show NO-binding constants in the 10^3–10^5 range,[12−15] whereas corresponding model complexes are oftentimes only stable in the presence of excess NO in solution. It is therefore believed that the protein matrix plays a significant role in stabilizing these species. As our work presented in this paper shows, this prominent conclusion is in fact incorrect.

The generally applied method for the preparation of ferric heme-NO complexes in the literature is the reaction of ferric heme precursors with weakly coordinated anions, [Fe(Porph)(X)] (X = BF_4^-, ClO_4^-, etc.; Porph = general porphyrin^{2-} ligand), with excess NO gas as shown in Scheme 1. This results in the formation of the respective five-coordinate (5C) ferric heme-nitrosyl complexes, [Fe(Porph)(NO)]X, and in the

Received: June 14, 2017

DOI: 10.1021/acs.inorgchem.7b01493
Inorg. Chem. XXXX, XXX, XXX–XXX

Scheme 1. Synthesis of Iron NO Complexes[a]

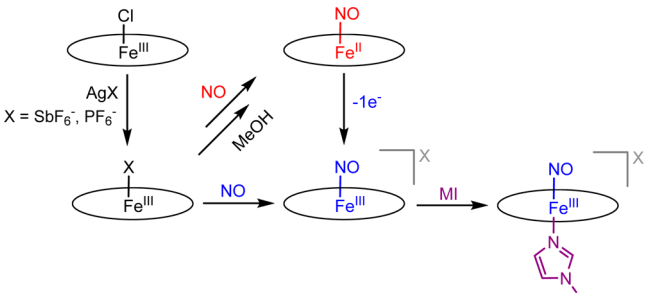

[a]MI = 1-methylimidazole. The oval represents the porphyrin ligand.

presence of an N-donor ligand (L), 6C complexes [Fe(Porph)(NO)(L)]X are formed. These $\{FeNO\}^6$ model systems are typically handled, stored, and redissolved under NO-saturated conditions due to their inherent propensity to lose NO from the iron center.[16−20] Also, using this method, the formed iron(III)−NO complexes react with any trace water (or bases such as methanol) in the presence of excess NO gas to form corresponding ferrous heme-NO, or $\{FeNO\}^7$, complexes. This process is called reductive nitrosylation and has been studied in detail in the literature.[21−23] This frequently results in isolated mixtures of $\{FeNO\}^{6/7}$ complexes. Despite these difficulties, several 5C and 6C ferric heme-nitrosyl complexes with the OEP^{2-} (octaethylporphyrin^{2-}) coligand were prepared and crystallized using this approach and characterized by UV−vis (in an NO atmosphere) and IR spectroscopy (in the solid state).[17,18,24−26] Besides OEP^{2-}, another synthetic porphyrin frequently applied in model complex studies is TPP^{2-} (tetraphenylporphyrin^{2-}). In the latter case, however, there are only four crystal structures of $\{FeNO\}^6$ complexes available: $[Fe(TPP)(NO)(H_2O)]^+$,[19,27] $[Fe(TpivPP)(NO)(NO_2)]$,[25] $[Fe(TPP)(NO)(CO_2CF_3)]$,[28] and $[Fe(TPP)(NO)(ROH)]^+$.[20] Since model complex studies performed in our and many other laboratories are heavily based on TPP^{2-} and its derivatives,[16,29−40] this represents a surprising knowledge gap in the literature.

In this work, we first prepared the $\{FeNO\}^6$ complexes $[Fe(TPP)(NO)]^+$ and $[Fe(TPP)(NO)(MI)]^+$ (MI = 1-methylimidazole) using the established literature method, and we fully characterized these compounds using UV−vis, IR, NMR, and nuclear resonance vibrational spectroscopy (NRVS). In addition, we obtained the first crystal structures for these complexes. We further devised a convenient route to synthesize these $\{FeNO\}^6$ complexes via chemical oxidation of the corresponding $\{FeNO\}^7$ precursor [Fe(TPP)(NO)], which can be accomplished by both chemical and electrochemical means as shown in Scheme 1. Using this method of preparation results in a surprisingly solution-stable 5C $\{FeNO\}^6$ complex that very slowly loses NO over a long period of time. With this notable stability, we also show that the oxidation of [Fe(TPP)(NO)] in the presence of ∼1 equiv MI generates the 6C $\{FeNO\}^6$ complex $[Fe(TPP)(NO)(MI)]^+$ in pure form. The $\{FeNO\}^6$ complexes generated via chemical oxidation have identical spectroscopic features to those made via the traditional method of preparation. The remarkable stability of the $\{FeNO\}^6$ complexes against NO loss observed here differs from many previous reports in the literature. The accelerated NO loss in the latter cases is probably due to halide impurities (although other impurities could certainly also play a role), and we demonstrate that addition of halide to solutions of our $\{FeNO\}^6$ complexes indeed leads to fast NO loss.

Furthermore, as previously discussed, $\{FeNO\}^7$ complexes are frequently synthesized by reductive nitrosylation (or commonly referred to as "autoreduction") of ferric precursors. In many cases, this reaction is started from a ferric chloride complex, [Fe(Porph)(Cl)], that is reacted with excess NO gas in the presence of base (such as methanol). In the first step of the proposed mechanism, the ferric chloride complex binds NO to form an intermediate, [Fe(Porph)(NO)(Cl)], which then reacts with the base resulting in a ferrous porphyrin complex (see Scheme 2). This autoreduction has been studied in detail,

Scheme 2. Proposed Reductive Nitrosylation Mechanism[a]

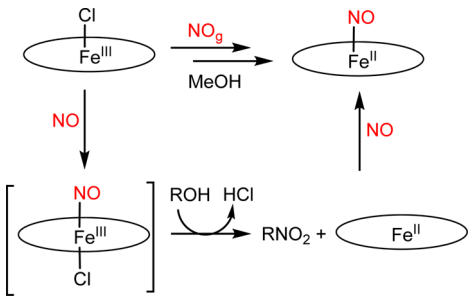

[a]Also known as autoreduction.

but there has been limited characterization of the elusive chloride-bound $\{FeNO\}^6$ intermediate.[41] To learn more about this process, we synthesized the complex [Fe(TPP)(NO)(Cl)] and characterized it using different spectroscopic methods. We found that this complex loses NO from the iron center very easily and needs to be handled under an NO-saturated atmosphere at all times. Finally, we also characterized this species using X-ray crystallography, which represents the first crystal structure of any [Fe(Porph)(NO)(Cl)] complex reported to this date.

EXPERIMENTAL PROCEDURES

All reactions were performed under inert conditions using Schlenk techniques. The preparation and handling of air-sensitive materials was carried out under a dinitrogen atmosphere in an MBraun glovebox equipped with a circulating purifier (O_2, H_2O < 0.1 ppm). Nitric oxide (Cryogenic Gases Inc., 99.5%) was purified by passage through an ascarite II column (NaOH on silica) followed by a cold trap at −80 °C to remove higher-order nitrogen oxide impurities. $^{15}N^{18}O$-Nitric oxide (Sigma-Aldrich) was used without further purification. All solvents (including deuterated solvents) and 1-methylimidazole (MI) were distilled from CaH_2 under dinitrogen and then degassed via five freeze−pump−thaw cycles. Tetrabutylammonium hexafluorophosphate was recrystallized from ethanol. The purified solvents were stored over appropriately sized activated molecular sieves in the glovebox until used. 1,1′-Diacetylferrocene was purchased from Fisher Scientific and used without any further purification. [Fe(TPP)(Cl)],[42] $[Fe(TPP)(X)]$[43] where X = PF_6^- or SbF_6^- and [thianthrene][X][44] where X = BF_4^- or SbF_6^- were synthesized as previously reported. ^{57}Fe complexes were synthesized in the same way as the natural abundance isotopes complexes, using $^{57}FeCl_2$ dimethanol salt as the iron source. All $\{FeNO\}^6$ complexes that are prepared from NO gas were precipitated under an NO atmosphere and then isolated in a dinitrogen atmosphere (in a glovebox).

Root-Mean-Square Deviation Determination. The root-mean-square deviation (RMSD) is calculated by the following equation:[7]

DOI: 10.1021/acs.inorgchem.7b01493
Inorg. Chem. XXXX, XXX, XXX−XXX

$$\mathrm{RMSD} = \sqrt{\frac{1}{N}\sum (\mathrm{dist})^2}$$

where N corresponds to the number of atoms that constitute the mean heme plane and dist is the distance (in Å) of a specific atom to the mean heme plane. The RMSD can be calculated from the 25-atom core displacement or the 4-atom *meso* carbon displacement.

Physical Measurements. Infrared spectra were obtained from KBr disks on PerkinElmer BX and GX spectrometers at room temperature. Measurements in solution were performed in a cell equipped with two CaF_2 windows on the same instruments. Electronic absorption spectra were measured using an Analytical Jena Specord S600 instrument at room temperature. In situ UV−vis measurements were taken with a Hellma quartz immersion probe with a 10 mm path length. Electron paramagnetic resonance spectra were recorded on a Bruker X-band EMX spectrometer equipped with Oxford Instruments liquid nitrogen and helium cryostats. EPR spectra were typically obtained on frozen solutions using 20 mW microwave power and 100 kHz field modulation with the amplitude set to 1 G. Sample concentrations were ∼1−3 mM. Proton and fluorine NMR spectra were recorded on a Varian MR 400 MHz instrument or a Varian NMRS 500 MHz spectrometer at room temperature. Cyclic voltammograms were obtained using a CH instruments CHI600E electrochemical workstation with a three-component electrochemical cell consisting of a glassy carbon working electrode, platinum counter electrode, and silver-wire pseudoreference electrode. All potentials were corrected to Fc/Fc^+. UV−vis and IR spectroelectrochemical (SEC) measurements were performed using custom-built thin-layer electrochemical cells as previously described.[30] All electrochemical and spectroelectrochemical measurements were carried out in the presence of 0.1−0.3 M tetrabutylammonium hexafluorophosphate. Nuclear resonance vibrational spectroscopy (NRVS) was carried out as previously described[45] at beamline 3-ID-XOR at the Advanced Photon Source (APS) at Argonne National Laboratory. This beamline provides about 2.5×10^9 photons/sec in ∼1 meV bandwidth (8 cm^{-1}) at 14.4125 keV in a 0.5 (vertical) × 0.5 mm (horizontal) spot. Samples were loaded into 4 × 7 × 1 mm copper cells. The final spectra represent averages of four scans. The program Phoenix was used to convert the NRVS raw data to the vibrational density of states (VDOS).[46,47] All of the $\{^{57}FeNO\}^6$/$\{^{57}Fe^{15}N^{18}O\}^6$ complexes were pure as determined by IR spectroscopy. The resonance Raman (rR) measurements were performed using the 413.13 nm excitation line from a Kr^+ ion laser (Spectra Physics Beam Lok 2060-RS). Raman spectra were recorded at 77 K using an Acton two-stage TriVista 555 monochromator connected to a liquid-nitrogen-cooled CCD camera (Princeton Instruments Spec-10:400B/LN). The total exposure time of the samples to the laser radiation was 3 min using 1−2 accumulations, and typical laser powers were in the 20−30 mW range.

Crystal Structure Determination. All crystals were measured on a Rigaku AFC10K Saturn 944+ CCD-based X-ray diffractometer equipped with a low-temperature device and a Micromax-007HF Cu-target microfocus rotating anode (λ = 1.54187 Å) operated at 1.2 kW power (40 kV, 30 mA). The X-ray intensities were measured at 85 K with the detector placed at a distance of 42.00 mm from the crystals.

[Fe(TPP)(NO)(MI)]PO_2F_2. A black needle of [Fe(TPP)(NO)(MI)]-PO_2F_2 of dimensions 0.22 × 0.05 × 0.02 mm was mounted on the diffractometer. A total of 4053 images were collected with an oscillation width of 1.0° in ω. The exposure time was 5 s for the low angle images, 30 s for high angle. The integration of the data yielded a total of 71 715 reflections to a maximum 2θ value of 136.44° of which 9081 were independent, and 6991 were greater than $2\sigma(I)$. The final cell constants (Table S1) were based on the xyz centroids of 18 806 reflections above $10\sigma(I)$. Analysis of the data showed negligible decay during data collection. The data were processed with CrystalClear 2.0 and corrected for absorption.[48] The structure was solved and refined with the Bruker SHELXTL (version 2008/4) software package,[49] using the space group $P\bar{1}$ with Z = 2 for the formulae $FeC_{48}H_{34}N_7O$, $PO_2F_2^-$, CH_2Cl_2, and H_2O. All non-hydrogen atoms were refined anisotropically with the hydrogen atoms placed in idealized positions. Full matrix least-squares refinement based on F^2 converged at R1 = 0.1099 and wR2 = 0.2727 [based on $I > 2\sigma(I)$], R1 = 0.1244 and wR2 = 0.2791 for all data. Additional details are presented in Tables S2−S6 and are given as Supporting Information.

[Fe(TPP)(NO)]BF_4. A brown block-like crystal of [Fe(TPP)(NO)]-BF_4 of dimensions 0.22 × 0.12 × 0.12 mm was mounted on the diffractometer. A total of 2028 images were collected with an oscillation width of 1.0° in ω. The exposure times were 5 s for the low-angle images and 30 s for high-angle images. Rigaku d*trek images were exported to CrysAlisPro for processing and corrected for absorption.[48,50] The integration of the data yielded a total of 64 490 reflections to a maximum 2θ value of 139.14° of which 15 452 were independent and 14 777 were greater than $2\sigma(I)$. The final cell constants (Table S7) were based on the xyz centroids of 30 783 reflections above $10\sigma(I)$. Analysis of the data showed negligible decay during data collection. The structure was solved and refined with the Bruker SHELXTL (version 2014/6) software package,[49] using the space group $P\bar{1}$ with Z = 4 for the formulae $FeC_{44}H_{28}N_5O$, BF_4^-, and $2.25(CH_2Cl_2)$. All non-hydrogen atoms were refined anisotropically with the hydrogen atoms placed in idealized positions. Full matrix least-squares refinement based on F^2 converged at R1 = 0.0714 and wR2 = 0.1969 [based on $I > 2\sigma(I)$], R1 = 0.0732 and wR2 = 0.1995 for all data. Additional details are presented in Table S8−S12 and are given as Supporting Information.

[Fe(TPP)(NO)(Cl)]. A brown prism of [Fe(TPP)(NO)(Cl)] of dimensions 0.16 × 0.10 × 0.10 mm was mounted on the diffractometer. A total of 2028 images were collected with an oscillation width of 1.0° in ω. The exposure times were 1 s for the low-angle images and 4 s for the high-angle images. Rigaku d*trek images were exported to CrysAlisPro for processing and corrected for absorption.[48,50] The integration of the data yielded a total of 13 642 reflections to a maximum 2θ value of 137.91° of which 870 were independent and 867 were greater than $2\sigma(I)$. The final cell constants (Table S13) were based on the xyz centroids of 6524 reflections above $10\sigma(I)$. Analysis of the data showed negligible decay during data collection. The structure was solved and refined with the Bruker SHELXTL (version 2014/6) software package,[49] using the space group $I4/m$ with Z = 2 for the formula $FeC_{44}H_{28}N_5OCl$. All non-hydrogen atoms were refined anisotropically with the hydrogen atoms placed in idealized positions. The chloro and nitrosyl ligands are disordered 50/50% on both faces of the porphyrin. Full matrix least-squares refinement based on F^2 converged at R1 = 0.0492 and wR2 = 0.1506 [based on $I > 2\sigma(I)$] and R1 = 0.0492 and wR2 = 0.1506 for all data. Additional details are presented in Tables S14−S19 and are given as Supporting Information.

Synthesis of [Fe(η^5-$C_5H_4COMe)_2$][BF_4]. In the glovebox, 115 mg (0.426 mmol) of 1,1′-diacetylferrocene and 129 mg (0.426 mmol) of [thianthrene][BF_4] were dissolved in 7 mL of dichloromethane, which caused a light-blue solid to precipitate from the reaction mixture. The reaction was allowed to stir for ∼30 min and, at this point, was vacuum filtered through a frit to give a teal blue powder. This powder was washed with dichloromethane and hexanes and then stored in the glovebox freezer. Yield: 93 mg (0.261 mmol, 61%). UV−vis (CH_2Cl_2): 655 nm. Anal. Calcd for $C_{14}H_{14}BF_4FeO_2$: C, 47.11; H, 3.95; N, 0.00. Found: C, 46.69; H, 3.58; N, 0.00. No peaks from the oxidant are observed in the ^1H NMR spectrum. $^{19}F\{^1H\}$ NMR (CD_2Cl_2, 377 MHz): −168.341 (s). IR (KBr): ν(CO) = 1693 cm^{-1}, $\nu(BF_4)$ = 1054 cm^{-1}.

Synthesis of [Fe(η^5-$C_5H_4COMe)_2$][SbF_6]. In the glovebox, 72 mg (0.267 mmol) of 1,1′-diacetylferrocene and 118.6 mg (0.262 mmol) of [thianthrene][SbF_6] were dissolved in 5 mL of dichloromethane, which caused a light-blue solid to precipitate from the reaction mixture. The reaction was allowed to stir for ∼30 min and, at this point, was vacuum filtered through a frit to give a teal blue powder. This powder was washed with dichloromethane and hexanes and then stored in the glovebox freezer. Yield: 59 mg (0.117 mmol, 44%). UV−vis (CH_2Cl_2): 655 nm. Anal. Calcd for $C_{14}H_{14}F_6FeO_2Sb$: C, 33.24; H, 2.79; N, 0.00. Found: C, 33.28; H, 2.71; N, 0.00. No peaks from the oxidant are observed in the ^1H NMR spectrum. $^{19}F\{^1H\}$ NMR (471 MHz): −123.96 (m). IR (KBr): ν(CO) = 1701 cm^{-1}, $\nu(SbF^6)$ = 659 cm^{-1}

DOI: 10.1021/acs.inorgchem.7b01493
Inorg. Chem. XXXX, XXX, XXX−XXX

Synthesis of [Fe(TPP)(NO)]. A 219 mg (0.242 mmol) portion of [Fe(TPP)(SbF_6)] was dissolved in 8 mL of dichloromethane and 1 mL of methanol. Then, the solution was exposed to NO gas, which caused the solution to turn bright red in color. The solution was brought carefully into the glovebox and allowed to stir overnight. The following day, 30 mL of methanol was added to the solution, which was then stored at −33 °C in the glovebox freezer. After 2 days, the reaction mixture was vacuum filtered in the glovebox through a frit, and the resulting dark-purple powder was washed with hexanes. Yield: 145 mg (0.208 mmol, 86%). UV−vis (CH_2Cl_2): 404, 476, 538, 612 nm. ^{1}H NMR (CD_2Cl_2, 400 MHz): δ = ∼ 6.0(br, β pyrrole H); 7.46 (s, *para*-H); 7.80 (br, *ortho*-H); 8.26 (s, *meta*-H). Peaks were assigned based on a previous literature report.[31] Anal. Calcd for $C_{44}H_{28}FeN_5O$ with 1 molecule of methanol: C, 73.98; H, 4.41; N, 9.59. Found: C, 73.99; H, 4.17; N, 9.78. IR (KBr): ν(NO) = 1696 cm^{-1}.

Synthesis of [Fe(TPP)(NO)]SbF_6. A 65 mg (0.0720 mmol) portion of [Fe(TPP)(SbF_6)] was dissolved in 4 mL of dichloromethane. Then, the solution was exposed to NO gas, which caused the solution to turn bright red in color. The solution was brought carefully into the glovebox and was layered with 20 mL of hexanes and stored at −33 °C in the glovebox freezer overnight. The next day, a purple solid was filtered off in the glovebox through a frit. The complex was stored in the glovebox freezer. Yield: 59 mg (0.0631 mmol, 88%). UV−vis (CH_2Cl_2): 370, 411, 550 nm. ^{1}H NMR (CD_2Cl_2, 500 MHz): δ = 7.70−7.876 (m). ^{19}F{^{1}H} NMR (471 MHz): −126.99 (br, m). IR (KBr): ν(NO) = 1850 cm^{-1} and ν(SbF_6) = 656 cm^{-1}.

Synthesis of [Fe(TPP)(NO)(MI)]SbF_6. A 63 mg (0.0697 mmol) portion of [Fe(TPP)(SbF_6)] with 5.6 μL of MI (0.0662 mmol) added was dissolved in 3 mL of dichloromethane. Then, the solution was exposed to NO gas, which caused the solution to turn bright red in color. The solution was brought carefully into the glovebox and was layered with 16 mL of hexanes and stored at −33 °C in the glovebox freezer overnight. The next day, a purple solid was filtered off in the glovebox through a frit. The complex was stored in the glovebox freezer. Yield: 45 mg (0.0442 mmol, 64%). UV−vis (CH_2Cl_2): 430, 544, 580 nm. IR (KBr): ν(NO) = 1918 cm^{-1} and ν(SbF_6) = 658 cm^{-1}. The corresponding PF_6^- complex (used for crystallization below) was prepared in a similar manner.

Synthesis of [Fe(TPP)(NO)(Cl)]. A 104 mg (0.148 mmol) portion of [Fe(TPP)(Cl)] was dissolved in 11 mL of dichloromethane. Then, the solution was exposed to NO gas, which caused the solution to turn brown-red in color. The solution was brought carefully into the glovebox and was layered with 30 mL of hexanes and stored at −33 °C in the glovebox freezer overnight. The next day, the resulting solid was filtered off in the glovebox through a frit. The complex was stored in the glovebox freezer. Yield: 40 mg (0.0545 mmol, 37%). UV−vis (CH_2Cl_2): 430, 544, 582 nm. IR (KBr): ν(NO) = 1880 cm^{-1}.

Synthesis of [Fe(TPP)(NO)(X)] using [TBA][X] (X = Cl^-, Br^-, I^-). [Fe(TPP)(SbF_6)] (61.3 mg, 0.068 mmol) was dissolved in 4 mL of dichloromethane and then exposed to NO gas, causing the solution to turn bright red in color. Then, the solution was carefully brought into the glovebox, and 22 mg of tetrabutylammonium bromide (0.0682 mmol), dissolved in 0.3 mL of dichloromethane, was injected into the solution, which was then allowed to stir for ∼30 min. Over time, the solution turned more brown-red in color, and at that point, the solution was layered with 15 mL of hexanes and left in the glovebox freezer. Several hours later, the solution was vacuum filtered to give a purple solid coated in a white patina (the white patina is [TBA][SbF_6]). IR (KBr): ν(NO) = 1870 cm^{-1}. The procedure with tetrabutylammonium chloride (ν(NO) = 1880 cm^{-1}) and tetrabutylammonium iodide was carried out in a similar manner. However, with [TBA][I], the ferric NO complex is reduced by one electron, forming [Fe(TPP)(NO)] (ν(NO) = 1696 cm^{-1}), I_2, and [TBA][SbF_6]. Typically, ∼1.0−1.3 equiv of the halide salt were used to do these experiments.

Chemical Oxidation of [Fe(TPP)(NO)]. Under an inert atmosphere, 6.6 mg of [Fe(TPP)(NO)] (0.0094 mmol) was dissolved in 3 mL of dichloromethane. The solution was added to 5.7 mg of solid [Fe(η^5-$C_5H_4COMe)_2$][SbF_6] (0.0113 mmol) and agitated until all of the solid had dissolved, forming [Fe(TPP)(NO)]SbF_6. The solution changed color from brown-red to bright red. EPR and solution IR data were recorded on the same sample to ensure full conversion and complete nitrosylation of the iron complex. No NO gas was added to the gas head space in these experiments. UV−vis (CH_2Cl_2): 370, 411, 550 nm. ^{1}H NMR (CD_2Cl_2, 400 MHz): δ = 7.25 (s); 7.46 (s); 7.72 (s); 7.88 (s). ^{19}F{^{1}H} NMR (471 MHz): −125.83 (br, m). IR (CH_2Cl_2): ν(NO) = 1850 cm^{-1}.

Addition of MI. Under an inert atmosphere, 6.6 mg of [Fe(TPP)(NO)] (0.0094 mmol) was dissolved with ∼0.75 μL of MI in 3 mL of dichloromethane. The solution was added to 5.7 mg of solid [Fe(η^5-$C_5H_4COMe)_2$][SbF_6] (0.0113 mmol) and agitated until all of the solid had dissolved, forming [Fe(TPP)(NO)(MI)]SbF_6. The solution changed color from brown-red to bright red. EPR and solution IR data were recorded on the same sample to ensure full conversion and complete nitrosylation of the iron complex. No NO gas was added to the gas head space in these experiments. Note: Samples of [Fe(TPP)(NO)(MI)]$^+$ generally contain a small amount of [Fe(TPP)(NO)]SbF_6, which is evident from a small solution-IR band at 1850 cm^{-1}. UV−vis (CH_2Cl_2): 430, 544, 580 nm. ^{1}H NMR (CD_2Cl_2, 400 MHz): δ = 2.06 (s); 3.90 (s); 4.68 (s); 7.26 (s); 7.49 (s); 7.83 (s); 8.14 (s); 9.16 (s). IR (CH_2Cl_2): ν(NO) = 1920 cm^{-1}.

Crystallization of [Fe(TPP)(NO)(MI)]PO_2F_2. [Fe(TPP)(NO)(MI)]-PF_6 (10 mg) (see discussion below regarding the counterion) was dissolved in 0.2 mL of NO-saturated dichloromethane and placed in a 5 mm diameter glass tube and sealed with a septa. The solution was then carefully layered with 2 mL of NO-saturated hexanes and placed in a −33 °C glovebox freezer. After 3 days, black needles suitable for X-ray analysis were collected.

It should be noted that in the crystal structure of this complex, the counterion is not the PF_6^- anion and was determined to be $PO_2F_2^-$ through a series of ^{31}P- and ^{19}F-NMR experiments. The $PO_2F_2^-$ counterion is formed during the methathesis reaction of the ferric chloride complex, [Fe(TPP)(Cl)], with $AgPF_6$ to form the ferric PF_6^- complex and AgCl. Interestingly, the PF_6^- anion further undergoes an iron-catalyzed hydrolysis (in the presence of trace amounts of water), resulting in a mixture of PF_6^- and $PO_2F_2^-$ counterions. This reaction has been noted in previous reports.[51,52] Initially, we did not observe the $PO_2F_2^-$ counterion in the bulk material of [Fe(TPP)(PF_6)] because it is bound to the iron center, and the paramagnetism of the iron center masks the signals in the NMR spectra. To counteract this problem, excess (>2 equiv) MI was added to the solution of the iron(III)−PF_6 complex to remove the $PO_2F_2^-$ ligand from the iron center (via formation of [Fe(TPP)$(MI)_2$]$^+$ and free $PO_2F_2^-$ and PF_6^-), which allowed us to observe the signals from both the PF_6^- and $PO_2F_2^-$ counterions in the ^{19}F- and ^{31}P NMR spectra (see Figures S4−S5).

Crystallization of [Fe(TPP)(NO)(Cl)]. [Fe(TPP)(Cl)] (55.6 mg) was dissolved in 6 mL of dichloromethane. Then, the solution was exposed to NO gas and brought carefully into the glovebox. Next, ∼0.2 mL of the solution was transferred to a 5 mm diameter glass tube and layered with 2 mL of dimethoxyethane (DME) and placed in a −33 °C glovebox freezer. After 4 days, brown prisms suitable for X-ray analysis were collected.

Crystallization of [Fe(TPP)(NO)]BF_4. A portion of [Fe(TPP)(NO)] (15.5 mg, 22.2 mmol) was dissolved in 3.5 mL of dichloromethane. To this solution, 9.9 mg of solid [DAcFc][BF_4] (27.7 mmol) was added, and the solution was agitated until the oxidant was completely dissolved. In a 5 mm diameter glass tube, 0.2 mL of the oxidized solution was carefully layered with 2 mL of hexanes and placed in a −33 °C glovebox freezer. After 3 days, brown block-like crystals suitable for X-ray analysis were collected. Excess NO gas was not required.

RESULTS AND ANALYSIS

Preparation of {FeNO}^{6} Complexes using NO Gas. Using standard literature procedures,[16,17] we reacted ferric porphyrins with the TPP^{2-} coligand, for example [Fe(TPP)-(SbF_6)], with excess NO gas to form the corresponding five-coordinate (5C) {FeNO}^{6} complex, [Fe(TPP)(NO)]SbF_6. In

DOI: 10.1021/acs.inorgchem.7b01493
Inorg. Chem. XXXX, XXX, XXX−XXX

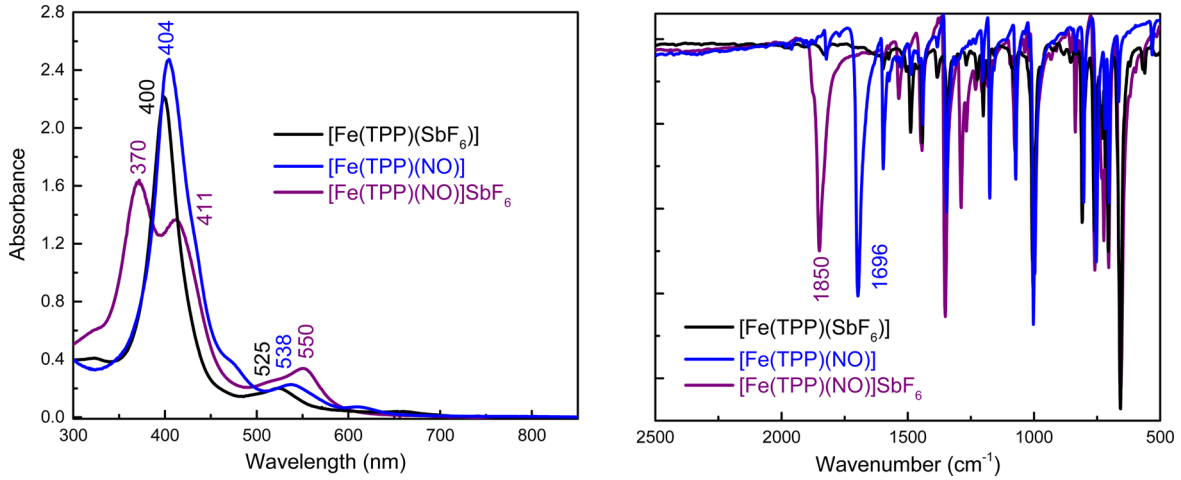

Figure 1. Left: Comparison of the UV−vis spectra of the precursor, [Fe(TPP)(SbF_6)] (black), the {FeNO}^{7} complex [Fe(TPP)(NO)] (blue), and the {FeNO}^{6} complex [Fe(TPP)(NO)]SbF_6 (purple, redissolved under non-NO-saturated conditions), isolated from the reaction of the iron(III)-SbF_6 complex with excess NO gas in dichloromethane. All spectra recorded at room temperature. Right: Overlay of the IR spectra of the precursor, [Fe(TPP)(SbF_6)] (black), [Fe(TPP)(NO)] (blue), and [Fe(TPP)(NO)]SbF_6 (purple) measured in KBr pellets.

the solid state, this compound has an N−O stretching frequency of 1850 cm^{-1} as shown in Figure 1 (right), which is consistent with the analogous OEP^{2-} complex (N−O stretching frequency is 1862 cm^{-1}).[19] The dissolution of the solid {FeNO}^{6} complex in dichloromethane (Figure 1, left) results in a UV−vis spectrum with a split Soret band at 370 and 411 nm and a Q-band at 550 nm. The ^{1}H NMR spectrum of the redissolved solid contains a multiplet of peaks from 7.70−7.88 ppm as shown in Figure S6, which is indicative of a diamagnetic iron heme complex, demonstrating that the complex is pure (NO loss results in a paramagnetic species). However, monitoring the solution over time by in situ UV−vis and solution IR experiments shows that the complex is not stable and shows signs of decomposition into a ferrous heme-nitrosyl complex after 2 h (Figure S24). The Fe−NO unit is reduced by a single electron, and the source of the electron is likely an impurity or potentially the solvent. Next, we synthesized the six-coordinate (6C) ferric heme-nitrosyl complex [Fe(TPP)(NO)(MI)]X (X = PF_6^-, SbF_6^-) and characterized this complex by UV−vis and IR spectroscopy. The UV−vis spectrum was obtained by reacting the ferric precursor complex with excess NO gas in the presence of ∼1 equiv of MI, resulting in features at 430, 544, and 580 nm (see Figure S7). The UV−vis spectrum of this {FeNO}^{6} complex is generally similar to that of [Fe(TpivPP)(NO)(NO_2)], previously reported by Scheidt and co-workers.[25] The IR of our 6C complex in the solid state shows a very intense N−O stretching frequency at 1918 cm^{-1} and no feature at 1676 cm^{-1}, which would indicate the presence of an {FeNO}^{7} impurity (see Figure S8). The dissolution of this {FeNO}^{6} complex in dichloromethane (see Figure S7), monitored by UV−vis spectroscopy, shows decomposition of the complex into a ferric bis-imidazole complex, [Fe(TPP)$(MI)_2$]SbF_6, and the ferric complex [Fe(TPP)(SbF_6)] via NO loss.

Preparation of {FeNO}^{6} Complexes via {FeNO}^{7} Oxidation. To overcome the problems with autoreduction and purity, we investigated an alternative route to synthesize ferric NO complexes that was inspired by previous studies by Kadish and co-workers.[53] In their work, cyclic voltammetry (CV) experiments on iron−NO complexes, such as [Fe(TPP)-(NO)], were performed, and it was found that the one-electron oxidation of this complex is chemically reversible. Additionally, IR and UV−vis SpectroElectroChemical (SEC) studies of the 5C {FeNO}^{7} complex showed clean formation of the oxidized product, for example [Fe(TPP)(NO)]$^+$, at least on the CV time scale. In the presence of ∼1 equiv of N-donor ligands (such as pyridine), [Fe(TPP)(NO)(Py)]$^+$ and analogous complexes were formed. However, attempts to obtain {FeNO}^{6} heme complexes on the preparative scale by bulk electrolysis of the {FeNO}^{7} precursors resulted in direct decomposition, generating a ferric porphyrin complex with a weakly coordinating anion (determined by UV−vis spectroscopy).[53] In fact, there is only one report in the literature (from 1995) that describes the successful generation of {FeNO}^{6} complexes via oxidation of {FeNO}^{7} precursors.[54] Since these pioneering studies, there have been no other attempts to synthesize {FeNO}^{6} complexes via one-electron oxidation of an {FeNO}^{7} precursor. With this in mind, we investigated the one-electron oxidation of the {FeNO}^{7} complex [Fe(TPP)(NO)], which itself was synthesized by reductive nitrosylation of [Fe(TPP)(SbF_6)] in a solution of methanol/dichloromethane that was exposed to excess NO gas. This reaction generates [Fe(TPP)(NO)] in pure form as determined by IR and ^{1}H NMR spectroscopy (see Figure S2). Next, we measured the CV of the {FeNO}^{7} complex as shown in Figure 2. The CV shows the {FeNO}$^{7/8}$ reduction at an $E_{1/2}$ value of −1.37 V vs Fc/Fc$^+$ in CH_2Cl_2, which is chemically reversible and consistent with the literature value of −1.42 V (vs Fc/Fc$^+$ in CH_2Cl_2).[30] The one-electron oxidation of the {FeNO}^{7} complex is observed at an $E_{1/2}$ value of +0.302 V vs Fc/Fc$^+$ in dichloromethane (+0.932 V vs NHE). The {FeNO}$^{7/6}$ oxidation is also chemically reversible, and our results are consistent with the literature ($E_{1/2}$ = +0.356 V vs Fc/Fc$^+$ in CH_2Cl_2).[53] In order to determine whether oxidation indeed produces the {FeNO}^{6} complex, [Fe(TPP)(NO)]$^+$, we then carried out the corresponding UV−vis and IR SEC studies on the {FeNO}^{7} complex. We can reversibly form the 5C {FeNO}^{6} complex by SEC, and the spectroscopic data are consistent with the literature reports (see Figure S16 for UV−vis SEC and Figure S17 for IR SEC) as well as the material that we obtained by reaction of [Fe(TPP)(X)] (X = PF_6^-, SbF_6^-) with NO gas (see above and Table 1). In particular, the IR SEC data show the

DOI: 10.1021/acs.inorgchem.7b01493
Inorg. Chem. XXXX, XXX, XXX−XXX

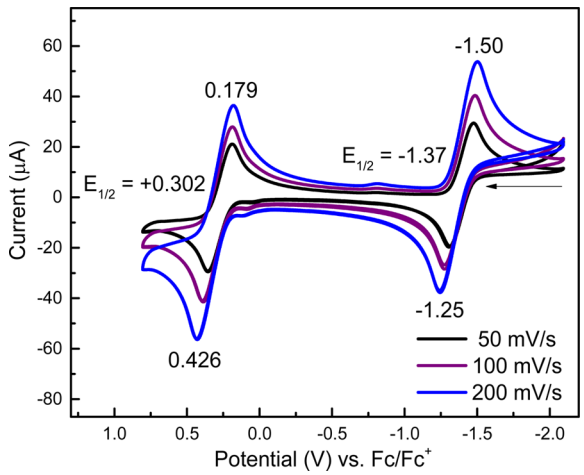

Figure 2. CV of ~6.6 mM [Fe(TPP)(NO)] in CH_2Cl_2 at room temperature. The working electrode was a glassy carbon electrode, and the counter electrode was a platinum electrode with an Ag wire pseudoreference. Tetrabutylammonium hexafluorophosphate was used as the electrolyte (~0.1 M).

N−O stretching vibration at 1676 cm^{-1} in the starting $\{FeNO\}^7$ complex (in CH_2Cl_2), which decreases in intensity upon oxidation as a new band at 1850 cm^{-1} appears. Additionally, the UV−vis and IR SEC oxidations were completed in the presence of ~1 equiv of MI (as a model for His in proteins). Whereas ferrous heme-NO complexes have a strong σ *trans* effect, leading to low binding constants of N-donor ligands to 5C ferrous heme-nitrosyls,[31] the corresponding ferric complexes do not show this effect.[14] Hence, in the SEC experiments, oxidation of the 5C $\{FeNO\}^7$ complex generates the corresponding 6C complex $[Fe(TPP)(NO)(MI)]^+$ in the presence of MI (UV−vis and IR SEC data for these transformations are shown in Figures S19,S20). In the IR SEC experiments, the N−O stretching vibration of [Fe(TPP)(NO)] at 1676 cm^{-1} disappears upon oxidation as new bands at 1920 and 1850 cm^{-1} appear (see Figure S20). The band at 1850 cm^{-1} corresponds to a small amount of the 5C $\{FeNO\}^6$ complex, $[Fe(TPP)(NO)]^+$.

Bulk Oxidation: A Better Way To Make Pure $\{FeNO\}^6$ Complexes. With spectroscopic handles on 5C and 6C $\{FeNO\}^6$ complexes with the TPP^{2-} coligand established, we investigated whether the bulk generation of these complexes is possible via one-electron chemical oxidation of the corresponding $\{FeNO\}^7$ precursor. The UV−vis spectra in Figure 3 show the titration of [Fe(TPP)(NO)] (in CH_2Cl_2 solution) with the chemical oxidant 1,1′-diacetylferrocenium hexafluoroantimonate ($E_{1/2}$ = +0.49 V vs Fc/Fc^+ in CH_2Cl_2),[55] abbreviated as $[DAcFc][SbF_6]$ (dissolved in dimethoxyethane (DME)), at room temperature. The reaction is complete with ~1 equiv of the oxidant, and the UV−vis data of the product exhibit features at 372, 404, and 550 nm that are identical to those of the UV−vis SEC-generated species (see overlay in Figure 4). The addition of excess ferrocene to the $\{FeNO\}^6$ solution reduces the complex back to the starting ferrous NO complex, as shown in the UV−vis spectra in Figure 4. The 5C $\{FeNO\}^6$ complex can also be generated at higher concentrations (2−6 mM range) for characterization by solution IR spectroscopy. For these experiments, the $\{FeNO\}^7$ complex, [Fe(TPP)(NO)], was dissolved in dichloromethane, and the resulting solution was then added to a slight excess of the solid oxidant, $[DAcFc][SbF_6]$, causing the solution to change color from orange-brown to bright red. The $\{FeNO\}^7$ precursor exhibits an intense N−O stretching vibration in dichloromethane at 1676 cm^{-1}, which shifts to 1850 cm^{-1} (Δ = 174 cm^{-1}) upon oxidation as shown in Figure 5. Intense C−O stretching bands from the $[DAcFc]^{0/+}$ oxidant are also observed in the IR spectrum at 1672 and 1702 cm^{-1}, respectively. Finally, we followed the conversion of the $\{FeNO\}^7$ precursor to the $\{FeNO\}^6$ species by EPR spectroscopy. EPR spectra at 4 K show that upon addition of the oxidant to the [Fe(TPP)(NO)] solution, an EPR-silent species is generated with a very minor high-spin ferric impurity that shows g values of ~5.7 (<5% from spin integration against [Fe(TPP)(Cl)]).

We further reacted the 5C $\{FeNO\}^6$ complex with ~1 equiv of MI to form the 6C complex $[Fe(TPP)(NO)(MI)]^+$. The UV−vis spectrum of $[Fe(TPP(NO)(MI)]^+$, shown in Figure S27, has features at 430, 544, and 580 nm, which matches the spectra of the complex made from iron(III)−X with excess NO gas and 1 equiv of MI, and also the UV−vis SEC-generated data (see Figure S28). On the basis of the UV−vis data shown in Figure S27, the $[Fe(TPP)(NO)(MI)]^+$ complex can also be formed by addition of ~1 equiv of MI to the $\{FeNO\}^7$ solution, followed by the addition of $[DAcFc][SbF_6]$ dissolved in DME. Figure 6 shows a comparison of the UV−vis spectra of all

Table 1. Comparison of Geometric Parameters for Selected $\{FeNO\}^6$ Complexes[a]

complex	Fe−N_p[b]	Fe−N(NO)	Fe−L	N−O	<Fe−N−O[c]	ref
$[Fe(TPP)(NO)]BF_4$	1.986/1.990	1.640(3)/1.665(3)	-	1.153(4)/1.124(4)	178.3(3)/177.4(3)	t.w.
$[Fe(OEP)(NO)]ClO_4$	1.994	1.644(3)	-	1.112(4)	176.9(3)	19
$[Fe(TPP)(NO)(MI)]PO_2F_2$	2.001	1.6275(3)	1.973(3)	1.148(5)	176.3 (4)	t.w.
$[Fe(TPP)(NO)(H_2O)]ClO_4$	1.999	1.652(5)	2.001(5)	1.150(2)	174.4(3)	19
$[Fe(TPP)(NO)(i\text{-}C_5H_{11}OH)]ClO_4$	2.013	1.776(5)	2.063(3)	0.925(6)	177.1(7)	20
$[Fe(OEP)(NO)(MI)]ClO_4$	2.003	1.6465(17)	1.9889(16)	1.135(2)	177.28(17)	17
$[Fe(OEP)(NO)(Pz)]ClO_4$	2.004	1.627(2)	1.988(2)	1.141(3)	176.9(3)	17
$[Fe(OEP)(NO)(Iz)]ClO_4$	1.996	1.632(3)	2.010(3)	1.136(4)	177.6(3)	17
[Fe(TPP)(NO)(Cl)]	2.011	1.668(9)	2.099(4)	1.209(8)	180	t.w.
$[Fe(TpivPP)(NO)(NO_2)]$[d]	1.996	1.671(2)	1.998(2)	1.144(3)	169.3(2)	25
$[Fe(TPP)(NO)(CO_2CF_3)]$	2.011	1.618(8)	1.899(6)	1.151(8)	175.8(6)	28
$[Fe(OEP)(NO)(SR\text{-}H_2)]$[e]	2.010	1.671(9)	2.356(3)	1.187(9)	159.6(8)	68

[a]Values for the bond distances given in Å and for the Fe−N−O angles given in degrees. The numbers given in parentheses are estimated standard deviations. A complete table of bond lengths and angles for crystal structures obtained in this work is given in the Supporting Information. [b]Average value. [c]All values are given in degrees. [d]TpivPP = *meso*-tetra($\alpha,\alpha,\alpha,\alpha$-o-pivalamidophenyl)porphyrin^{2-}. [e]SR-H_2 = S-2,6-$(CF_3CONH)_2C_6H_3$.

DOI: 10.1021/acs.inorgchem.7b01493
Inorg. Chem. XXXX, XXX, XXX−XXX

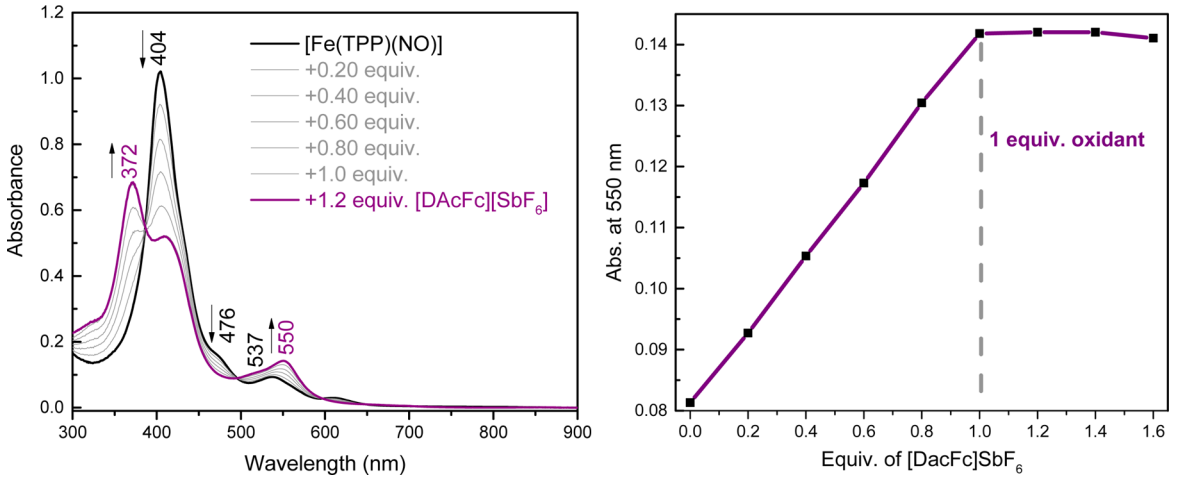

Figure 3. Left: UV−vis spectra following the titration of ∼10 μM [Fe(TPP)(NO)] (black) with the chemical oxidant [DAcFc][SbF_6] (dissolved in dimethoxyethane) in dichloromethane, forming the ferric NO complex $[Fe(TPP)(NO)]^+$ (purple). Right: Changes of the absorption at 550 nm upon addition of the oxidant, showing that the reaction is complete after the addition of one equiv of oxidant.

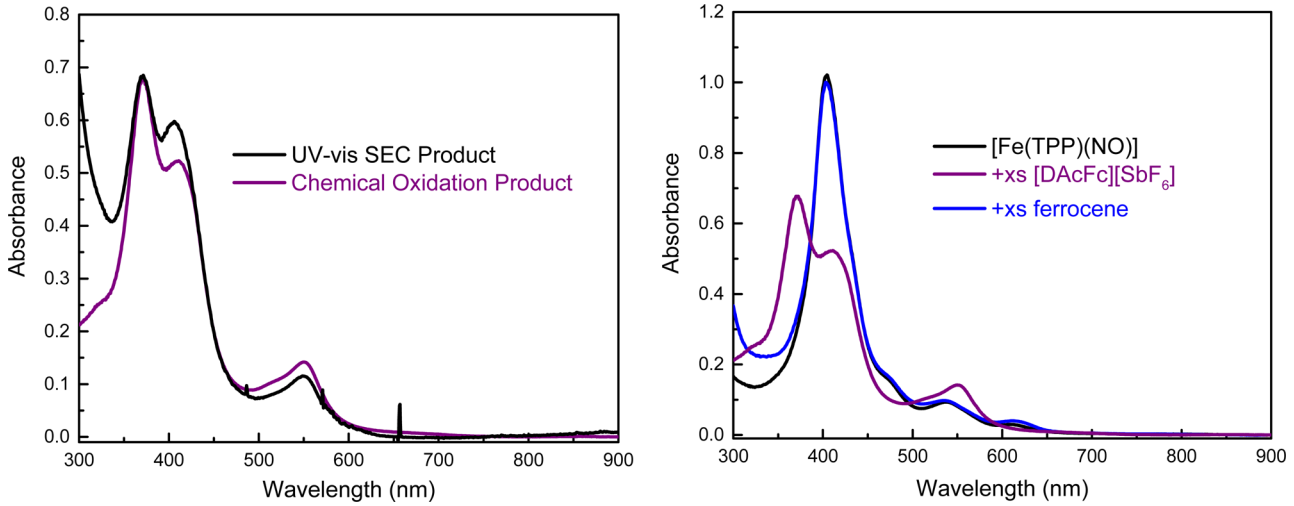

Figure 4. Left: UV−vis SEC used for the formation of $[Fe(TPP)(NO)]^+$ (black), compared to $[Fe(TPP)(NO)]^+$ (purple) generated by chemical oxidation, both recorded in dichloromethane. These data show that identical species are formed by both methods. Right: UV−vis spectra of [Fe(TPP)(NO)] before (black) and after addition of the chemical oxidant [DAcFc][SbF_6] (dissolved in dimethoxyethane) in dichloromethane, leading to the formation of the ferric NO complex, $[Fe(TPP)(NO)]^+$ (purple). Subsequent reaction of the oxidized species with ferrocene reforms the $\{FeNO\}^7$ precursor (blue).

relevant complexes. For the preparation of 2−6 mM solutions, the $\{FeNO\}^7$ complex, [Fe(TPP)(NO)], was dissolved in dichloromethane with ∼1 equiv of MI, and the resulting solution was then added to a slight excess of the solid oxidant, [DAcFc][SbF_6], causing the solution to change color from orange-brown to deep red with a pink hue. The $\{FeNO\}^7$ precursor exhibits an intense N−O stretching band in dichloromethane at 1676 cm^{-1}, which shifts to 1920 cm^{-1} (Δ = 244 cm^{-1}) upon oxidation in the presence of MI as shown in Figure S29. The small band at 1850 cm^{-1} can be attributed to the $[Fe(TPP)(NO)]^+$ complex. As previously mentioned, intense C−O stretching bands from the $[DAcFc]^{0/+}$ oxidant are also observed in the IR spectrum at 1672 and 1702 cm^{-1}, respectively. Lastly, the conversion to the $\{FeNO\}^6$ complex was quantified by EPR spectroscopy. The oxidation product is EPR silent with only a small (<5%) high-spin ferric heme impurity (integrated against [Fe(TPP)(Cl)]).

In summary, we have established a convenient method to make preparative amounts of ferric heme-nitrosyl complexes via chemical oxidation of iron(II)−NO precursors at room temperature and characterized all products using different spectroscopic methods.

Stability of the $\{FeNO\}^6$ Complex. As mentioned above, the generally used literature method to synthesize both 5C and 6C ferric NO model complexes frequently results in inherently unstable species in solution that have a high propensity to lose NO over time (in the absence of excess NO gas). This is surprising, considering that analogous 6C ferric heme-NO complexes in protein active sites (where the proximal ligand is a histidine or cysteinate) are quite stable under NO-limited conditions.[12] The instability of the $\{FeNO\}^6$ heme model complexes makes studies of their fundamental properties and reactivity difficult in solution, since such studies require the presence of excess NO gas, which by itself is very reactive and can interfere with the desired reactivity studies. In contrast to these previous observations, we noticed that the $\{FeNO\}^6$ complexes, when generated via oxidation of the corresponding $\{FeNO\}^7$ precursors, are surprisingly stable. To investigate this

DOI: 10.1021/acs.inorgchem.7b01493
Inorg. Chem. XXXX, XXX, XXX−XXX

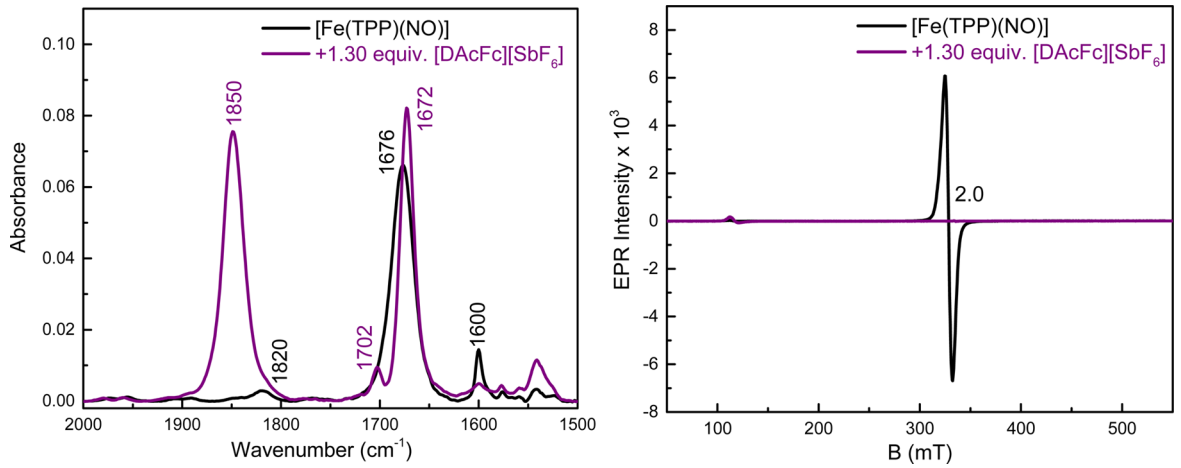

Figure 5. Left: Solution IR spectra of 1.8 mM [Fe(TPP)(NO)] (black) in CH_2Cl_2 and of the reaction product (purple) after the addition of ~1.30 equiv of $[DAcFc][SbF_6]$ added to the solution. The N−O stretch at 1676 cm^{-1} shifts to 1850 cm^{-1} upon oxidation. The bands at 1702 and 1672 cm^{-1} are the C−O stretching frequencies (ester groups) of the respective $DAcFc^{0/+}$ reagents. Right: EPR spectra of the same solutions used for the solution IR experiments (on the left) at 4 K. The black spectrum represents the $\{FeNO\}^7$ complex with a broad, isotropic $S = 1/2$ signal at $g = 2.0$, and the purple spectrum represents the solution of the corresponding oxidized species, $[Fe(TPP)(NO)]^+$, which is EPR silent and contains a minor $g = 6$ signal that spin integrates to <5% of a ferric impurity. The sample was spin integrated against [Fe(TPP)(Cl)] using SpinCount.

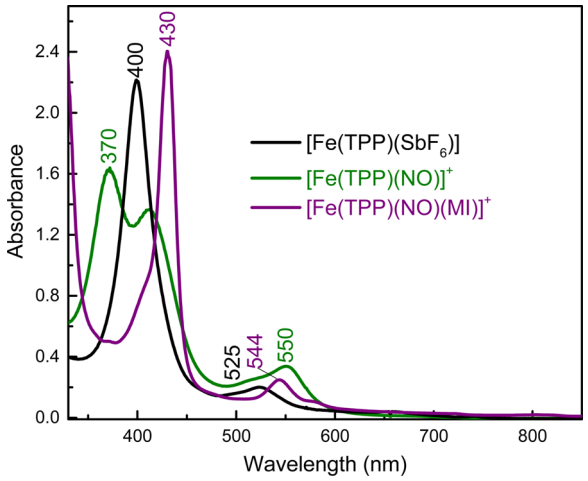

Figure 6. Comparison of the UV−vis spectra of the five-coordinate $\{FeNO\}^6$ complex $[Fe(TPP)(NO)]^+$ (green), the six-coordinate complex $[Fe(TPP)(NO)(MI)]^+$ (purple), and the $[Fe(TPP)(SbF_6)]$ precursor (black) in dichloromethane. All spectra recorded at room temperature.

further, we took aliquots from the oxidation-reaction solutions and monitored the changes in the IR spectra over a ~24 h time period at room temperature. After a few hours, the N−O stretching band at 1850 cm^{-1} of the 5C complex completely overlaid with the initial IR spectrum, indicating minimal NO loss (see Figure S21). After >15 h, the 1850 cm^{-1} band starts to slowly decrease in intensity; however, this change is very small, indicating that the $\{FeNO\}^6$ complex is quite stable in solution in the absence of excess NO. At the same time, the intensity of the C−O stretching band of reduced DAcFc at 1672 cm^{-1} increases notably. Since excess $[DAcFc][SbF_6]$ oxidant is present in solution, we tested whether $[DAcFc][SbF_6]$ is stable in DME (the oxidant is not soluble enough in dichloromethane for solution IR measurements). The IR spectra in Figure S22 show that the oxidant $[DAcFc][SbF_6]$ decomposes within 2 h to form DAcFc and other decomposition products. Therefore, we believe that the increasing intensity of the band at 1672 cm^{-1} can be attributed to excess oxidant that decomposes over time. Another possibility is that some amount of $\{FeNO\}^7$ complex is formed over time. This complex shows the N−O stretch at 1676 cm^{-1}, which could contribute to the intensity increase of the 1672 cm^{-1} feature. In order to test this further, EPR spectroscopy was used (Figure S23). In order to ensure consistency, we used the same solutions for solution IR and EPR spectroscopy (Figures S21,S23). At cryogenic temperatures of ~4 K, the $\{FeNO\}^7$ precursor has a broad $S = 1/2$ signal with a g value centered at 2.0 (note: when the temperature is raised to 77 K, the hyperfine couplings from the ^{14}N atom of NO appear; see Figure S18), and the addition of a slight excess of $[DAcFc][SbF_6]$ results in a completely EPR-silent spectrum as shown in Figure S23. Over time (t > 15 h), a small signal around g = ~ 6 appears in the EPR spectrum, which is indicative of a hs ferric heme complex resulting from NO loss. Spin integration of this signal against [Fe(TPP)(Cl)] shows that it corresponds to <5% ferric complex. No formation of the $\{FeNO\}^7$ complex is observed. In conclusion, the 5C $\{FeNO\}^6$ complex is stable over extended periods of time in solution as shown by UV−vis, solution IR, and EPR spectroscopy. Analysis of the UV−vis data in Figure S33 estimates the k_{off} rate of NO for $[Fe(TPP)(NO)]^+$ to be ~4.7 × 10^{-5} s^{-1}. For the six-coordinate adduct, $[Fe(TPP)(NO)(MI)]^+$, we monitored the stability of the complex by solution IR experiments as shown in Figure S34. Over ~6 h, a decrease in the intensity of NO band of the complex at 1920 cm^{-1} is observed, and an increase in the band at 1850 cm^{-1} from the five-coordinate complex, $[Fe(TPP)(NO)]^+$, is noted. The imidazole complex, $[Fe(TPP)(MI)]^+$, has an extremely high binding affinity for another MI ligand, resulting in the bis-imdazole complex, $[Fe(TPP)(MI)_2]^+$.[56] This corresponds to the reaction sequence in eqs 1,2. Analysis of the UV−vis data after the addition of MI to a solution of $[Fe(TPP)(NO)]^+$ results in a significantly larger k_{off} of ~1.9 × 10^{-4} s^{-1} (Figure S35) than that of $[Fe(TPP)(NO)]^+$ (Figure S33). The observed rate constant for $[Fe(TPP)(NO)(MI)]^+$ compares favorably with ferric heme NO complexes in protein environments, which have k_{off} rate constants that range from ~10^1−10^{-2} s^{-1} (this includes Mb/Hb, NPs, HRP, NOS, and Cyt.

DOI: 10.1021/acs.inorgchem.7b01493
Inorg. Chem. XXXX, XXX, XXX−XXX

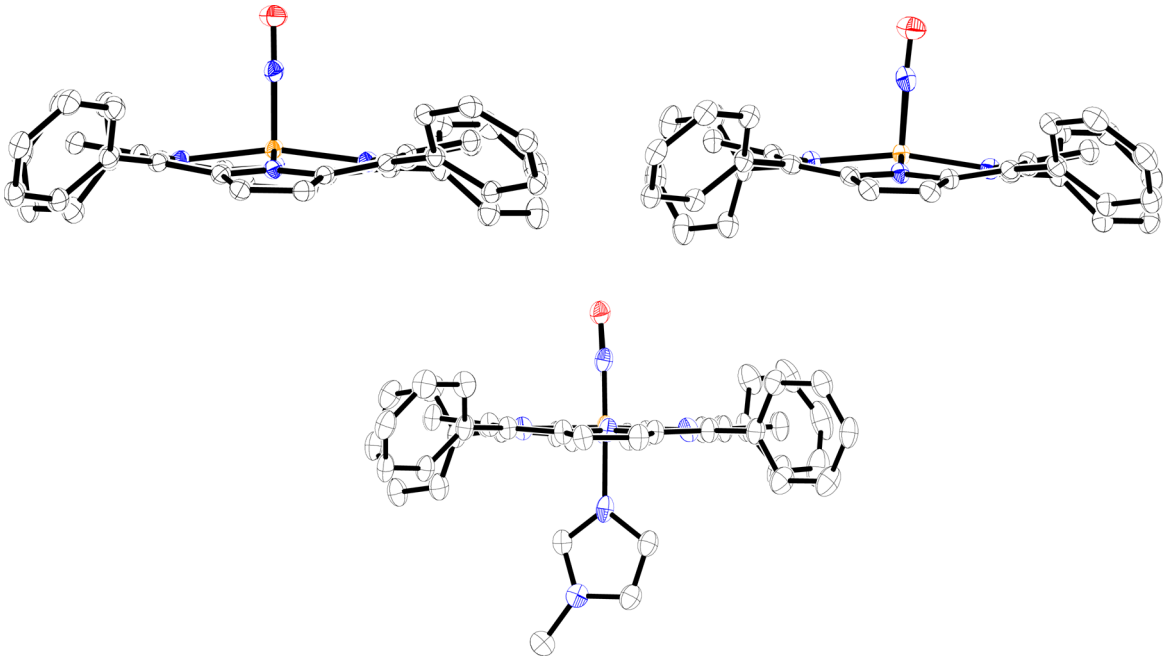

Figure 7. Top: Crystal structures of the two different 5C {FeNO}^{6} complexes in the unit cell of [Fe(TPP)(NO)]BF_4. Bottom: Crystal structure of [Fe(TPP)(NO)(MI)]PO_2F_2. In all structures, the hydrogen atoms, solvent molecules, and counterions are omitted for clarity. Thermal ellipsoids are shown at 40% probability.

P450s; Mb denotes myoglobin, Hb denotes hemoglobin, HRP denotes horseradish peroxidase, and NPs denotes nitrophorins).[12] In contrast, previous work with other model complexes shows much faster k_{off} rates of $\sim 10^1$–10^3 s^{-1} (see, for example, ref 57).

$$[Fe(TPP)(NO)(MI)]^+ \xrightarrow{k_1} [Fe(TPP)(MI)]^+ + NO \quad (1)$$

$$[Fe(TPP)(MI)]^+ + [Fe(TPP)(NO)(MI)]^+ \xrightarrow{k_2} [Fe(TPP)(MI)_2]^+ + [Fe(TPP)(NO)]^+ \quad (2)$$

Crystallographic Studies. With the long-term stability of $[Fe(TPP)(NO)]^+$ in solution established, we prepared the 5C {FeNO}^{6} complex as described above from the chemical oxidant, [DAcFc][BF_4] and then layered the solution with hexanes and placed it in the −33 °C freezer to obtain X-ray quality crystals (in the absence of excess NO gas). The crystal structure of [Fe(TPP)(NO)]BF_4 is shown in Figure 7. In the unit cell, there are two unique {FeNO}^{6} complexes with slightly different geometric parameters (see Table 1). The crystal structure of the complex exhibits a linear Fe−N−O unit (Fe−N−O angle: 177.4(3)/178.3(3)°) and Fe−NO bond lengths of 1.640/1.665 Å. These bond lengths are in agreement with the crystal structure of [Fe(OEP)(NO)]ClO_4, which exhibits an Fe−NO bond length of 1.644 Å.[19] Interestingly, the porphyrin is completely planar in the crystal structure of the 5C {FeNO}^{6} complex with the OEP^{2-} coligand, but the heme plane is ruffled in our crystal structure of [Fe(TPP)(NO)]BF_4. A ruffling distortion is characterized by the rotation of *trans* pyrrole rings in the opposite direction around the Fe−$N_{pyrrole}$ bonds of the porphyrin coligand. This distortion is commonly observed in 5C ferric porphyrins because the iron sits above the heme plane. This out-of-plane distortion is measured by the RMSD of the porphyrin atoms from the heme plane. The 25-atom core displacement of [Fe(TPP)(NO)]BF_4 is 0.31 Å, whereas planar hemes are defined by a 25-atom core displacement of less than 0.10 Å.[7] For example, the completely planar complex [Fe(TMP)$(MI)_2$]ClO_4 (TMP^{2-} = tetramesitylporphyrin) has a 25-atom core displacement of 0.02 Å,[58] which is 15 times smaller than that of [Fe(TPP)(NO)]BF_4. The RMSD for the 4-atom *meso* carbon displacement of [Fe(TPP)(NO)]BF_4 is 0.077 Å. In addition, we crystallized the analogous {FeNO}^{6} complex with MI bound to the iron center. The bulk material, [Fe(TPP)(NO)(MI)]PF_6, was prepared by reaction of the ferric precursor with excess NO gas in dichloromethane. The dissolution of [Fe(TPP)(NO)(MI)]PF_6 in dichloromethane, layered with hexanes under an NO atmosphere, at −33 °C, results in needle-like crystals. The crystal structure of this complex is shown in Figure 7. It should be noted that the counterion in this structure is $PO_2F_2^-$ as further discussed in the Experimental Procedures. This is the first crystal structure of a 6C ferric heme-nitrosyl complex with an N-donor ligand using TPP^{2-} as the porphyrin. In the crystal structure of [Fe(TPP)(NO)(MI)]PO_2F_2, the porphyrin coligand is completely planar, unlike the ruffled conformation of the heme in the 5C complex [Fe(TPP)(NO)]BF_4. The complex exhibits a linear Fe−N−O unit (Fe−N−O angle: 176.3(4)°), and the Fe−NO bond length is 1.628 Å, which is similar to other 6C ferric heme-nitrosyl complexes with neutral N-donor ligands that exhibit Fe−NO bond lengths ranging from 1.627−1.647 Å (Table 1).[17] It should be noted that this {FeNO}^{6} complex has a Fe−N_{MI} bond length of 1.973 Å, which is slightly shorter than those in other neutral N-donor coordinated {FeNO}^{6} complexes with the OEP^{2-} coligand, which show Fe−N bond lengths ranging from 1.996−2.003 Å as shown in Table 1. Finally, the average Fe−$N_{pyrrole}$ bond distance is 2.001 Å, similar to other 6C ferric heme-nitrosyl complexes.[17]

Role of Halides for Stability. With a stable 5C {FeNO}^{6} complex in hand, we further investigated the stability of this complex in the presence of halides. First, we generated the {FeNO}^{6} complex via chemical oxidation of the {FeNO}^{7} precursor with [DAFc][SbF_6], and then reacted it with ∼1

DOI: 10.1021/acs.inorgchem.7b01493
Inorg. Chem. XXXX, XXX, XXX−XXX

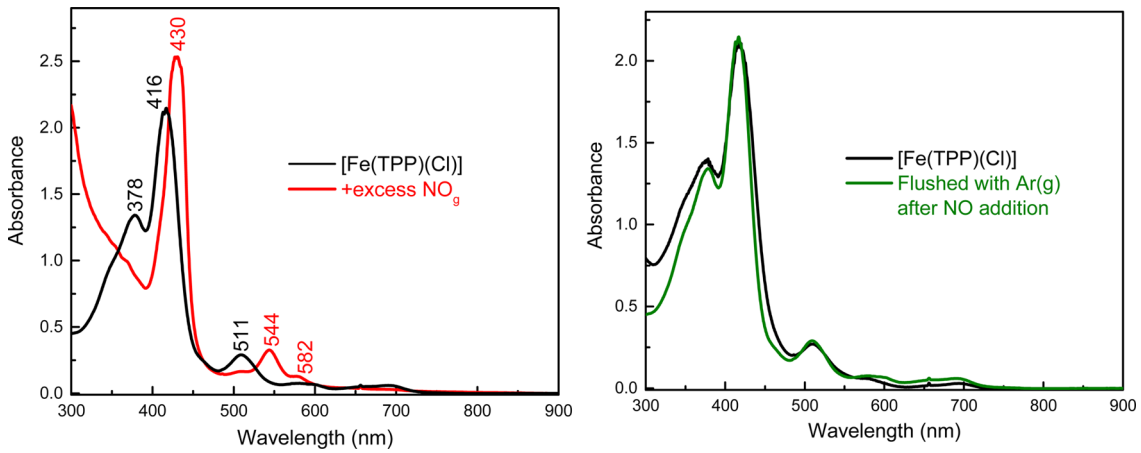

Figure 8. Left: UV−vis spectra of the ferric precursor, [Fe(TPP)(Cl)] (black) and of the corresponding reaction product after bubbling the solution with NO(g) to form [Fe(TPP)(NO)(Cl)] (red), in CH_2Cl_2. Right: The reaction product after flushing the solution with argon gas (green), which results in reformation of the starting material [Fe(TPP)(Cl)] (black).

equiv of tetrabutylammonium chloride (TBACl) and monitored the reaction using in situ UV−vis spectroscopy. Addition of [TBA][Cl] to the {FeNO}^{6} solution results in immediate formation of the ferric chloride complex [Fe(TPP)(Cl)] and NO release as shown in Figure S9. The same result is also obtained when $[Fe(TPP)(NO)]^+$ is reacted with [TBA][Br] forming a ferric bromide complex (Figure S9). This is consistent with previous work by Wayland and co-workers and shows that the {FeNO}^{6} complex, [Fe(TPP)(NO)(Cl)], is not stable under non-NO-saturated conditions. In this work, it was observed that SEC-generated [Fe(Porph)(NO)(X)] complexes (where X = Cl^-, Br^-, and I^-) were unstable and decomposed into the corresponding [Fe(Porph)(X)] complexes.[52] However, at low temperature (−70 °C), the addition of [TBA][Br] to the {FeNO}^{6} solution results in the formation of a new species with a Soret band at 435 nm and the main Q-band at 550 nm (see Figure S11, top). This species has features that are consistent with a six-coordinate {FeNO}^{6} complex. When the solution is warmed to room temperature, this species rapidly decomposes into [Fe(TPP)(Br)] within 5 min as shown in Figure S11 (bottom).

Quest for the Elusive Complex [Fe(TPP)(Cl)(NO)]—The Critical Intermediate in Reductive Nitrosylation. Ferrous heme-nitrosyl complexes, {FeNO}^{7}, are typically synthesized by reductive nitrosylation as mentioned in the Introduction. In reductive nitrosylation, a ferric precursor complex, [Fe(Porph)(X)] (where $Porph^{2-}$ = a $porphyrin^{2-}$ coligand; X^- = monoanionic ligand: halide, PF_6^-, SbF_6^-, ClO_4^-, etc.), is typically reacted with excess NO gas in the presence of a base (such as methanol).[59] In the first step of the proposed mechanism, a ferric chloride complex, for example, binds NO to the iron center to form a 6C ferric heme-nitrosyl complex, [Fe(Porph)(NO)(Cl)], which then reacts with the base to form HCl, RNO_2, and a ferrous porphyrin complex (see Scheme 1). The ferrous heme then binds another equivalent of NO to generate the respective {FeNO}^{7} complex.[12] The key intermediate for this process, [Fe(Porph)(NO)(Cl)], has so far only been poorly characterized in the literature. In a previous report from over 30 years ago, Wayland and co-workers describe the reaction of [Fe(TPP)(Cl)] with excess NO gas to form [Fe(TPP)(NO)(Cl)], monitored by in situ UV−vis spectroscopy. The isolated reaction product was characterized in the solid state by IR spectroscopy.[41] Additionally, Kadish and co-workers carried out the IR SEC oxidation of [Fe(TPP)(NO)] in the presence of [TBA][Cl], [TBA][Br], and [TBA][I], resulting in the potential formation of the corresponding {FeNO}^{6} complexes [Fe(TPP)(NO)(X)] where X = Cl^-, Br^-, and I^-. The N−O stretching frequencies of these complexes were reported to occur at 1886, 1883, and 1879 cm^{-1}, respectively.[53] We generated [Fe(TPP)(NO)(Cl)] by reacting the ferric chloride complex with excess NO gas. Under an NO atmosphere, hexanes were added to precipitate the target complex. Characterization of the isolated complex in the solid state by IR spectroscopy shows an N−O stretching frequency of 1880 cm^{-1} (Figure S12, left). This ferric chloride NO complex shows minimal NO loss over a 3 month time period in the solid state when stored in the glovebox freezer at −33 °C (Figure S12, right). The dissolution of the NO complex results in immediate NO loss from the iron center and reformation of the ferric chloride precursor. Due to the facile NO loss from the iron center, the ferric chloride complex, [Fe(TPP)(Cl)], was reacted with excess NO gas in dichloromethane directly in a Schlenk cuvette in order to obtain the UV−vis spectrum of [Fe(TPP)(NO)(Cl)]. The resulting spectrum shows features at 430, 544, and 582 nm (Figure 8) that are similar to the spectral features observed for the 6C {FeNO}^{6} complex $[Fe(TPP)(NO)(MI)]^+$ (see Figure 6). Upon flushing the cuvette with argon gas, the ferric chloride precursor is reformed, indicating again that NO binding is reversible (Figure 8, right). In addition, under an NO-rich environment, we were able to grow crystals of [Fe(TPP)(NO)(Cl)] and solve the crystal structure of this complex, which is displayed in Figure 9. It should be noted that the crystal structure is disordered with respect to the NO and Cl^- ligands, which makes the heme plane appear atypically planar. The crystal structure of this complex exhibits a linear Fe−N−O unit (Fe−N−O angle: 180°), an Fe−NO bond length of 1.6685 Å, and an Fe−Cl distance of 2.013 Å (the Fe−Cl bond length in [Fe(TPP)(Cl)] is 2.192 Å).[60]

Finally, we reacted the 5C {FeNO}^{6} complex with other halides to form the corresponding halide-bound complexes, [Fe(TPP)(NO)(X)], X = Br^-, I^- under an NO-saturated atmosphere. The reaction of $[Fe(TPP)(NO)]^+$ with [TBA][Br] results in the corresponding bromide-coordinated NO complex, [Fe(TPP)(NO)(Br)], and [TBA][SbF_6]. The N−O stretching frequency of [Fe(TPP)(NO)(Br)] is 1870 cm^{-1} as

DOI: 10.1021/acs.inorgchem.7b01493
Inorg. Chem. XXXX, XXX, XXX−XXX

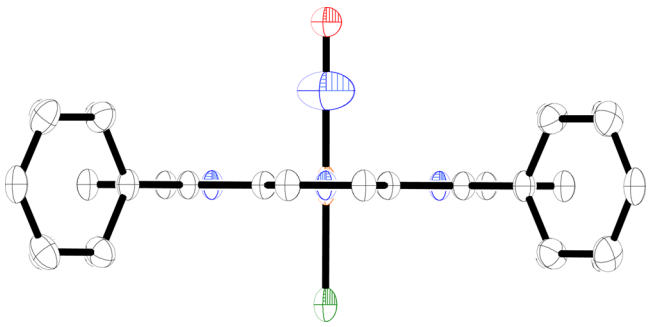

Figure 9. Crystal structure of [Fe(TPP)(NO)(Cl)]. The hydrogen atoms are omitted for clarity, and thermal ellipsoids are shown at 40% probability.

shown in Figure S11. Interestingly, in our hands, the reaction of $[Fe(TPP)(NO)]^+$ with [TBA][I] results in reduction of the Fe−N−O unit to form the ferrous-heme nitrosyl complex, [Fe(TPP)(NO)] (N−O stretching frequency = 1696 cm^{-1}), I_2, and [TBA][SbF_6] (see Figure S14). Furthermore, when a solution of $[Fe(TPP)(NO)]^+$ in dichloromethane in the absence of NO gas is reacted with [TBA][I], there is immediate formation of the [Fe(TPP)(NO)] complex as shown in Figure S15, indicating that iodide reduces the $\{FeNO\}^6$ complex in an outer sphere process (since no NO loss is observed).

Nuclear Resonance Vibrational Spectroscopy (NRVS). To gain further insight into the electronic properties of our new $\{FeNO\}^6$ complexes, we measured their Fe−NO stretching frequencies applying NRVS. In correlation to the N−O stretching frequencies, this provides key insight into changes in Fe−NO bonding along a series of complexes as we and others have previously shown.[16,31,61−64] In linear $\{FeNO\}^6$ complexes, the Fe−N−O unit gives rise to one Fe−NO stretch and two degenerate Fe−N−O linear bends, which, in the case of corresponding six-coordinate complexes, are very similar in energy.[16,24] This complicates spectral assignments.

The NRVS data of the 5C $\{FeNO\}^6$ complex, [^{57}Fe(TPP)(NO)]SbF_6, show the Fe−N−O bends at 393 cm^{-1}, which shift to 386 cm^{-1} upon $^{15}N^{18}O$ labeling (Δ = 7 cm^{-1}). This finding is fully consistent with the results for [Fe(OEP)(NO)]ClO_4, where the linear Fe−N−O bends are found at 402 cm^{-1}. At higher energy, there are two peaks observed at 559 and 585 cm^{-1} that are isotope sensitive. As shown in Figure 10, the spectrum of the $^{15}N^{18}O$ complex exhibits a significant decrease in the intensity of the peak at 585 cm^{-1}, while at the same time, the peak at 559 cm^{-1} increases in intensity. This implies that the Fe−NO stretch is located at 585 cm^{-1} and coupled with a porphyrin-based vibration around 559 cm^{-1}. This is consistent with work by Scheidt and co-workers on [Fe(OEP)(NO)]ClO_4 where the Fe−NO stretch is observed at 595 cm^{-1}. This would also explain the very large (apparent) isotope shift (Δ = 26 cm^{-1}) observed for this mode.

We also obtained NRVS data for the 6C complex, [^{57}Fe(TPP)(NO)(MI)]SbF_6, which show one isotope-sensitive feature at 590 cm^{-1} that downshifts to 573 cm^{-1} upon $^{15}N^{18}O$ labeling (Δ = 17 cm^{-1}). This complex exhibits a much sharper Fe−NO band in the NRVS spectrum than that of [Fe(TPP)(NO)(MI)]BF_4, as reported by us previously,[16] but again, the Fe−NO stretch and the Fe−N−O bends are not resolved (see ref 24). In the 6C case, we measured the resonance Raman (rR) spectrum of the [Fe(TPP)(NO)(MI)]SbF_6 complex. For this purpose, the precursor [Fe(TPP)(SbF_6)] was dissolved in

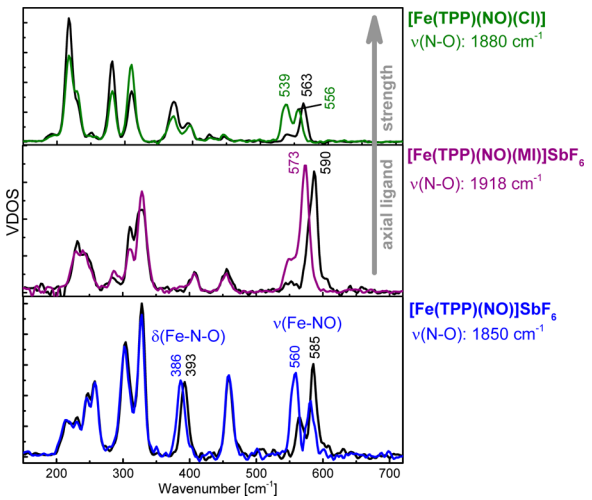

Figure 10. Top: NRVS-derived vibrational density of states (VDOS) for [^{57}Fe(TPP)(NO)(Cl)] (black) and the $^{15}N^{18}O$-labeled complex (green). Middle: NRVS VDOS for [^{57}Fe(TPP)(NO)(MI)]SbF_6 (black) and the $^{15}N^{18}O$-labeled complex (purple). Bottom: NRVS VDOS for [^{57}Fe(TPP)(NO)]SbF_6 (black) and the $^{15}N^{18}O$-labeled complex (blue).

dichloromethane in the presence of ∼1 equiv of MI and was exposed to NO gas. The NO-saturated solution was then transferred to a quartz EPR tube. In the rRaman spectrum shown in Figure S36, the oxidation-state marker band (ν_4) is observed at 1370 cm^{-1}, and the spin-state marker band (ν_2) is found at 1569 cm^{-1}, both consistent with other ferric heme-NO complexes.[65,66] Interestingly, the ν_4 and ν_2 bands are identical to the $\{FeNO\}^7$ complex [Fe(TPP)(NO)] (ν_4 = 1370, ν_2 = 1568 cm^{-1}), indicating that the heme is in the low-spin ferrous state.[31] In the low-energy region of the spectrum, the natural abundance isotopes (n.a.i.) complex exhibits a broad band at ∼598 cm^{-1} (see Figure S37, top) that downshifts to 586 cm^{-1} (Δ = 12 cm^{-1}) upon isotope labeling with $^{15}N^{18}O$ gas (Figure S37, bottom). In contrast to our complex, six-coordinate ferric heme-NO adducts in proteins (such as myoglobin) show resolved Fe−NO stretching and bending modes (measured via rRaman; see Table 2).[63]

Finally, in the [^{57}Fe(TPP)(NO)(Cl)] complex, the IR spectrum of the n.a.i. species show two isotope-sensitive features, the main band at 1880 cm^{-1} and a minor feature at 1829 cm^{-1} (see Figure S40). Isotope labeling with $^{15}N^{18}O$ results in a downshift of the N−O stretching frequency to 1802 cm^{-1} (Δ = 78 cm^{-1}), whereas the 1829 cm^{-1} feature actually shifts to higher energy at 1844 cm^{-1} (Δ = 15 cm^{-1}). We believe this is due to Fermi resonance, since the 1829/1844 cm^{-1} band is lower in energy than the N−O stretch in the n.a.i. complex, but higher in energy than the N−O stretch in the $^{15}N^{18}O$-labeled complex. The NRVS spectrum contains one isotope-sensitive band at 563 cm^{-1}, which shifts to 556 cm^{-1} upon $^{15}N^{18}O$ labeling (Δ = 7 cm^{-1}). There is another band at 539 cm^{-1} in the n.a.i. complex that significantly increases in intensity in the $^{15}N^{18}O$-labeled complex, indicating that the Fe−NO stretch is coupled to another vibration that is close in energy. We believe that this feature at 539 cm^{-1} is a Fe-porphyrin-related vibration that steals some intensity from the Fe−NO stretch. In summary, we can resolve the Fe−NO stretch from the linear Fe−N−O bends in the 5C complex, [Fe(TPP)(NO)]SbF_6; however, both 6C $\{FeNO\}^6$ complexes only show one combined band for these features.

DOI: 10.1021/acs.inorgchem.7b01493
Inorg. Chem. XXXX, XXX, XXX−XXX

Table 2. Comparison of Vibrational Frequencies for Selected {FeNO}^{6} Complexes

complex	ν(N−O) cm^{-1}	ν/δ(Fe−NO) cm^{-1}	ref
[Fe(TPP)(NO)]SbF_6	1850	δ: 393, ν: 585	t.w.
[Fe(OEP)(NO)]ClO_4	1862	δ: 402, ν: 595	19
[Fe(TPP)(NO)(MI)]SbF_6	1920	589	t.w.
[Fe(TPP)(NO)(MI)]BF_4	1896	δ: 586, ν: 578	16
[Fe(TPP)(NO)(H_2O)]ClO_4	1862	-	19
[Fe(TPP)(NO)(*i*-$C_5H_{11}OH$)]ClO_4	1935	-	20
[Fe(OEP)(NO)(MI)]ClO_4	1921	-	17
[Fe(OEP)(NO)(2-MI)]ClO_4	N/A	δ: 574, 580 ν: 600	17
[Fe(OEP)(NO)(Pz)]ClO_4	1909	-	17
[Fe(OEP)(NO)(Iz)]ClO_4	1914	-	17
Mb(III)−NO	1927	δ: 572, ν: 595	65, 74, 75
Hb(III)−NO	1925	594	65, 76, 77
rNP1(III)−NO	1917	δ: 578, ν: 591	66, 78
[Fe(TPP)(NO)(Cl)]	1880	563	t.w.
[Fe(TPP)(NO)(Br)]	1870	-	t.w.
[Fe(TpivPP)(NO)(NO_2)]ClO_4	1874	-	25
[Fe(TPP)(NO)(CO_2CF_3)]	1907	-	28
[Fe(OEP)(NO)(SR-H_2)][a]	1850	549	67, 68
[Fe(SPorph)(NO)][b]	1828	510	12
[Fe(SPoprh-HB)(NO)][c]	1837	515	12
P450nor(III)−NO	1851	530	71
P450cam(III)−NO	1806	528	70, 71
P450cam(III)−NO + camphor	1806	522	71, 72
P450cam(III)−NO + norcamphor	1818	524	71, 72
P450cam + adamantanone	1818	520	71, 72
CPO(III)−NO[d]	1868	538	71, 73

[a]SR−H_2 = S-2,6-$(CF_3CONH)_2C_6H_3$; [b]SPorph = *meso-a,a,a,a*-[o-[[(acetylthio)methyl]phenoxy]acetamido]phenyl]tris(o-pivalamidophenyl)porphyrin^{2-} [c]SPorph-HB = SPorph with proposed hydrogen bonding; [d]CPO denotes chloroperoxidase.

DISCUSSION

In this Article, we describe a convenient route to synthesizing ferric heme-nitrosyl complexes (without anionic axial ligands) in bulk by chemical and electrochemical oxidation of {FeNO}^{7} precursors in the absence of NO gas, and demonstrate this approach for complexes with the TPP^{2-} ligand. When generated in this way, the 5C {FeNO}^{6} complex is solution stable and slowly loses NO over time. The k_{off} rate is ∼4.7 × 10^{-5} s^{-1}, which means that the half-life is ∼4 h (see Figure S33). The addition of ∼1 equiv of MI (1-methylimidazole) to the solution results in the formation of the 6C complex $[Fe(TPP)(NO)(MI)]^+$, which is also solution stable, but shows a significantly enhanced rate for NO loss (k_{off} = ∼ 1..9 × 10^{-4} s^{-1} with a half-life of ∼1 h; see Figure S35). These rate constants for NO loss compare favorably with the values derived for proteins, which fall in the range of 10^1−10^{-2} s^{-1}, but are much smaller than typical values reported for model complexes, 10^1−10^3 s^{-1}.[12] This implies that it is not necessarily the protein matrix that is responsible for the enhanced stability of {FeNO}^{6} complexes in proteins but on the contrary, that there could also be factors that reduce the stability of these complexes in model systems. Our results show that one such source of instability are halide impurities: upon addition of ∼1 equiv of a chloride or bromide source to our {FeNO}^{6} complexes, immediate denitrosylation of the complexes is observed. With respect to *R. proxlixus* nitrophorins, this indicates that a special stabilization of the {FeNO}^{6} complexes by the protein matrix may not be required as previously proposed,[7] in particular since the saliva of *R. proxlixus* contains excess NO. Once the nitrophorins are injected into the victim's blood, the conformational changes of the protein (triggered by the change in pH) and the presence of histamine that can bind in the active site might actually be required to induce efficient NO loss.

We further characterized our series of {FeNO}^{6} complexes via UV−vis, IR, NMR, and NRVS. The {FeNO}^{6} complexes obtained in this way have identical spectroscopic features to those prepared via the traditional method shown in Scheme 1. The complexes are also more stable, which is likely due to less impurities in the precursor complex, especially halides. We avoid halide impurities by synthesizing a pure form of the {FeNO}^{7} complex via a reductive nitrosylation reaction from an iron(III)−X precursor (where X^- is a weakly coordinating anion). This approach allows us to handle {FeNO}^{6} complexes in the absence of any excess NO gas, enabling reactivity studies with reagents that are sensitive to NO gas (for example thiols).

Next, we determined that [Fe(TPP)(NO)(Cl)] can be made and isolated as a solid material. This complex represents the proposed key intermediate in the reductive nitrosylation of [Fe(Porph)(Cl)] and related ferric precursors (see Scheme 2), which is the most widespread method to prepare ferrous heme-nitrosyl complexes. Yet, not much is known about the properties of these types of complexes. [Fe(TPP)(NO)(Cl)] reversibly binds NO, but quickly loses NO upon dissolution of the isolated material or removal of excess NO gas from the reaction vessel. We can also generate the halide-bound {FeNO}^{6} complexes by addition of [TBA][X] (where X = Cl^- or Br^-) to a solution of $[Fe(TPP)(NO)]^+$ under an NO atmosphere. However, the reaction of [TBA][I] with $[Fe(TPP)(NO)]^+$ results in one-electron reduction of the Fe−NO unit to generate the ferrous heme-nitrosyl complex, [Fe(TPP)(NO)]. This finding is not in agreement with a previous literature report that presents the IR SEC oxidation of [Fe(TPP)(NO)] in the presence of [TBA][I], which was thought to result in the generation of [Fe(TPP)(NO)(I)] with an N−O stretching frequency of 1879 cm^{-1}.[53] To further elucidate this issue, we can examine the reduction potentials of the reported species in CH_3CN: for redox couples Cl^-/Cl_2, Br^-/Br_2, and I^-/I_2, redox potentials of +0.18, +0.07, and −0.14 V (vs Fc/Fc^+), respectively,[55] have been determined. Given the $E_{1/2}$ value of +0.302 V (vs Fc/Fc^+) for the {FeNO}^{6} complex (in dichloromethane), the oxidation potential of I^- to I_2 is roughly ∼440 mV more negative than the $[Fe(TPP)(NO)]/[Fe(TPP)(NO)]^+$ couple, which means the complex will easily oxidize I^- to I_2. This is also consistent with the fact that the ferric complex FeI_3 does not exist (due to conversion to FeI_2 + I_2). We speculate that the putative complex "[Fe(TPP)(NO)(I)]" reported previously is likely the nitro−nitrosyl complex [Fe(TPP)(NO)(NO_2)], which readily forms in the presence of O_2, is quite stable, and shows a similar N−O stretch of about 1875−1880 cm^{-1}.[16]

We further obtained the crystal structures for our new series of {FeNO}^{6} complexes. The 5C complex, [Fe(TPP)(NO)]BF_4, has a linear Fe−N−O unit (Fe−N−O angle: 177.4(3)/178.3(4)°) and a similar Fe−NO bond length of 1.640/1.665 Å compared to that of the [Fe(OEP)(NO)]ClO_4 complex (see Table 1). The only notable difference between these complexes

DOI: 10.1021/acs.inorgchem.7b01493
Inorg. Chem. XXXX, XXX, XXX−XXX

is that our 5C {FeNO}^{6} complex has a slightly lower N−O stretching frequency of 1850 cm^{-1} in comparison to the OEP^{2-} analogue at 1862 cm^{-1} (see Table 2).[19] The Fe−NO stretching and bending vibrations are observed at 585 and 393 cm^{-1}, which are slightly lower in energy than those of the [Fe(OEP)(NO)]ClO_4 complex at 595 and 402 cm^{-1}, respectively (see Table 2).[19] This indicates that the Fe(TPP) fragment is less electron-rich compared to Fe(OEP), leading to a weaker Fe−NO π backbond in the former, and correspondingly, a lower Fe−NO stretching frequency. Ferric heme-nitrosyl complexes with axial neutral N-donors (ie. imidazole, pyridine, and pyrazole) also have linear Fe−N−O units and N−O and Fe−NO stretching frequencies in the 1890−1935 cm^{-1} and 580−600 cm^{-1} range.[11] Our 6C complex [Fe(TPP)(NO)(MI)]$^+$ exhibits a linear Fe−N−O moiety (Fe−N−O angle: 176.3(4)°; see Table 1) with N−O and Fe−NO stretching-frequency values of 1920 and ∼589 cm^{-1} (see Table 2). Interestingly, ferric heme-nitrosyl species with histidine ligation, such as myoglobin/hemoglobin and nitrophorins, have N−O (1917−1927 cm^{-1}) and Fe−NO stretching frequencies (591−595 cm^{-1}) similar to those of our 6C N-donor {FeNO}^{6} complex (see Table 2). We have previously investigated the complex [^{57}Fe(TPP)(NO)(MI)]BF_4 with BF_4^- as the counterion (compared to SbF_6^- used here for NRVS). In this case, the NRVS data exhibit a broad, ^{15}N^{18}O-sensitive feature at 578/586 cm^{-1}.[16] In conjunction with normal coordinate analysis (NCA) and density functional theory (DFT) calculations, we assigned the Fe−NO stretch to the 578 cm^{-1} band and the Fe−N−O linear bends to the feature at 586 cm^{-1}. Further work by Scheidt and co-workers utilized oriented single-crystal NRVS to provide definitive assignments of the stretching and bending modes of the Fe−N−O moiety in the ^{57}Fe-labeled complexes [Fe(OEP)(NO)]ClO_4 and [Fe(OEP)(MO)(2-MI)]ClO_4 (2-MI = 2-methylimidazole).[24] These data show the Fe−NO stretch at higher energy than the Fe−N−O linear bends. This implies that for [Fe(TPP)(NO)(MI)]$^+$, the Fe−NO stretch should likely be identified with the mode at 586 cm^{-1}, reversing our previous assignment. This is supported by the resonance Raman data, which show the Fe−NO stretch at 598 cm^{-1} with natural abundance Fe in solution.

Interestingly, for six-coordinate {FeNO}^{6} complexes with anionic axial ligands, a correlation of the ligand donor strength and the Fe−N−O bond angle has been derived.[67] For example, with a weak donor like trifluoroacetate, [Fe(TPP)(NO)(CO_2CF_3)] exhibits a slightly bent Fe−N−O unit of 176°.[28] Upon increasing the donor strength, the Fe−N−O unit bends in [Fe(TpivPP)(NO)(NO_2)] with an Fe−N−O bond angle of 169°.[25] Furthermore, in the presence of an S-donor, [Fe(OEP)(NO)(SR-H_2)] (where SR-H_2 = S-2,6-$(CF_3CONH)_2C_6H_3$), the Fe−N−O moiety is bent even more at 160°.[68] By comparison, our chloride-bound {FeNO}^{6} complex, [Fe(TPP)(NO)(Cl)], has a linear Fe−N−O unit (180°), which would make Cl^- a very weak donor by this classification (similar to the acetate-ligated complex). However, the axial-ligand donor strength is also correlated with N−O and Fe−NO stretching frequencies as depicted in Figure 11. Interestingly, [Fe(TPP)(NO)(Cl)] falls in the region between the neutral N-donor- and thiolate-ligated complexes on the graph. This would indicate that the Cl^- ligand is a moderate donor but does not explain the fact that the Fe−N−O unit is completely linear. The most notable difference between the anionic ligands mentioned above is that they are all anisotropic

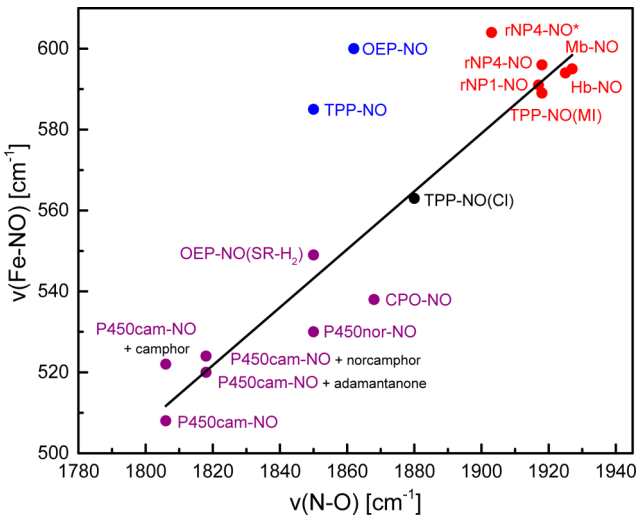

Figure 11. Experimental vibrational stretching frequency correlation of the Fe−NO versus the N−O stretching frequency based on this work and published data. 5C {FeNO}^{6} complexes [Fe(TPP)(NO)]BF_4 and [Fe(OEP)(NO)]ClO_4 are depicted in blue. 6C {FeNO}^{6} complexes with an axial thiolate ligand *trans* to NO are shown in purple: Cyt. P450cam[70,71] (+camphor, norcamphor, and adamantanone),[71,72] Cyt. P450nor,[71] CPO,[71,73] and [Fe(OEP)(NO)(SR-H_2)]ClO_4.[67,68] [Fe(TPP)(NO)(Cl)] is shown in black and 6C {FeNO}^{6} complexes with an axial histidine (Mb,[65,74,75] Hb,[65,76,77] and rNP[66,78]) or MI ligand *trans* to NO are shown in red. MI denotes 1-methylimidazole, SR-H_2 denotes the S-2,6-$(CF_3CONH)_2C_6H_3$ ligand, CPO denotes chloroperoxidase, Mb denotes myoglobin, Hb denotes hemoglobin, and rNP denotes nitrophorins from *Rhodnius prolixus*.

π-donors with one dominant lone pair, whereas chloride is the only isotropic π-donor with two equivalent Cl(p) π-donor orbitals. Previously, we have shown that thiolates cause a bending of the Fe−N−O unit by inducing a σ−trans effect on the bound NO via the population of an Fe−N−O σ^* antibonding orbital.[69] Our results for [Fe(TPP)(NO)(Cl)] show that this bending is also related to anisotropic π-donation, which is a fact that has previously been overlooked. Therefore, the Cl^- ligand is a moderate σ- and isotropic π-donor that causes a simultaneous weakening of the Fe−NO and N−O bonds, as demonstrated by vibrational spectroscopy, but the isotropic π-donating ability of Cl^- results in the linearity of the Fe−N−O unit unlike other anisotropic π-donor ligands. This emphasizes the importance of (vibrational) spectroscopy over structural data for the characterization of metal−ligand bond strength. More work is required to fully understand the electronic reasons for Fe−N−O bending in thiolate-coordinated ferric heme-NO complexes and the significance of this effect for NO activation in Cyt. P450s (especially Cyt. P450 NO reductase).[11]

In summary, our approach to synthesize {FeNO}^{6} complexes in the absence of excess NO gas makes future reactivity studies feasible with reagents that would typically react with free NO gas in solution. We spectroscopically and structurally characterized the 5C complex, [Fe(TPP)(NO)]$^+$ and the 6C complexes [Fe(TPP)(NO)(MI)]$^+$ and [Fe(TPP)(NO)(Cl)] with axial imidazole and halide coordination. The latter complex is a key intermediate in reductive nitrosylation that has never been properly characterized. Finally, we determined the k_{off} rates for NO loss from the different complexes prepared here, which emphasizes the ability of halides to denitrosylate {FeNO}^{6} complexes.

DOI: 10.1021/acs.inorgchem.7b01493
Inorg. Chem. XXXX, XXX, XXX−XXX

■ ASSOCIATED CONTENT

Supporting Information

The Supporting Information is available free of charge on the ACS Publications website at DOI: 10.1021/acs.inorgchem.7b01493.

The SI includes UV−vis, NMR, NRVS, rRaman, EPR, and FT-IR spectra (PDF)

Accession Codes

CCDC 1556645−1556647 contain the supplementary crystallographic data for this paper. These data can be obtained free of charge via www.ccdc.cam.ac.uk/data_request/cif, or by emailing data_request@ccdc.cam.ac.uk, or by contacting The Cambridge Crystallographic Data Centre, 12 Union Road, Cambridge CB2 1EZ, UK; fax: +44 1223 336033.

■ AUTHOR INFORMATION

Corresponding Author

*E-mail: lehnertn@umich.edu

ORCID

Nicolai Lehnert: 0000-0002-5221-5498

Notes

The authors declare no competing financial interest.

■ ACKNOWLEDGMENTS

This work was supported by a grant from the National Science Foundation (CHE-1464696 to N.L.). A.B.M. acknowledges a Rackham Merit Fellowship and the Wayne & Carol Pletcher Graduate Research Fellowship (University of Michigan). This research used resources of the Advanced Photon Source, a U.S. Department of Energy (DOE) Office of Science User Facility operated for the DOE Office of Science by Argonne National Laboratory under Contract No. DE-AC02-06CH11357.

■ REFERENCES

(1) Moncada, S.; Palmer, R. M.; Higgs, E. A. Nitric oxide: physiology, pathophysiology, and pharmacology. *Pharmacol. Rev.* **1991**, *43*, 109.

(2) Bredt, D. S.; Snyder, S. H. Nitric Oxide: A Physiologic Messenger Molecule. *Annu. Rev. Biochem.* **1994**, *63*, 175−195.

(3) Snyder, S. H. Nitric oxide: first in a new class of neurotransmitters. *Science* **1992**, *257*, 494.

(4) Stuehr, D. J. Structure-Function Aspects in the Nitric Oxide Synthases. *Annu. Rev. Pharmacol. Toxicol.* **1997**, *37*, 339−359.

(5) Li, H.; Poulos, T. L. Structure−function studies on nitric oxide synthases. *J. Inorg. Biochem.* **2005**, *99*, 293−305.

(6) Ignarro, L. J. Haem-dependent activation of cytosolic guanylate cyclase by nitric oxide: a widespread signal transduction mechanism. *Biochem. Soc. Trans.* **1992**, *20*, 465.

(7) Walker, F. A. Nitric oxide interaction with insect nitrophorins and thoughts on the electron configuration of the {FeNO}^{6} complex. *J. Inorg. Biochem.* **2005**, *99*, 216−236.

(8) Enemark, J. H.; Feltham, R. D. Principles of Structure, Bonding, and Reactivity for Metal Nitrosyl Complexes. *Coord. Chem. Rev.* **1974**, *13*, 339−406.

(9) Ferguson, S. J. Nitrogen cycle enzymology. *Curr. Opin. Chem. Biol.* **1998**, *2*, 182−193.

(10) Richardson, D. J.; Watmough, N. J. Inorganic nitrogen metabolism in bacteria. *Curr. Opin. Chem. Biol.* **1999**, *3*, 207−219.

(11) McQuarters, A. B.; Wirgau, N. E.; Lehnert, N. Model complexes of key intermediates in fungal cytochrome P450 nitric oxide reductase (P450nor). *Curr. Opin. Chem. Biol.* **2014**, *19*, 82−89.

(12) Lehnert, N.; Berto, T. C.; Galinato, M. G. I.; Goodrich, L. E. In *The Handbook of Porphyrin Science*; Kadish, K. M., Smith, K. M., Guilard, R., Eds.; World Scientific: Hackensack, NJ, 2011; Vol. *14*, pp 1−247.

(13) Cooper, C. E. Nitric oxide and iron proteins. *Biochim. Biophys. Acta, Bioenerg.* **1999**, *1411*, 290−309.

(14) Hoshino, M.; Ozawa, K.; Seki, H.; Ford, P. C. Photochemistry of nitric oxide adducts of water-soluble iron(III) porphyrin and ferrihemoproteins studied by nanosecond laser photolysis. *J. Am. Chem. Soc.* **1993**, *115*, 9568−9575.

(15) Lehnert, N.; Scheidt, W. R.; Wolf, M. W. In *Nitrosyl Complexes in Inorganic Chemistry, Biochemistry and Medicine II*; Mingos, D. M. P., Ed.; Springer Berlin Heidelberg: Berlin, Germany, 2014; pp 155−223.

(16) Praneeth, V. K. K.; Paulat, F.; Berto, T. C.; DeBeer George, S.; Näther, C.; Sulok, C. D.; Lehnert, N. Electronic Structure of Six-Coordinate Iron(III)-Porphyrin NO Adducts: the Elusive Iron(III)-NO(radical) State and Its Influence on the Properties of these Complexes. *J. Am. Chem. Soc.* **2008**, *130*, 15288−15303.

(17) Ellison, M. K.; Scheidt, W. R. Synthesis, Molecular Structures, and Properties of Six-Coordinate [Fe(OEP)(L)(NO)]$^+$ Derivatives: Elusive Nitrosyl Ferric Porphyrins. *J. Am. Chem. Soc.* **1999**, *121*, 5210−5219.

(18) Ellison, M. K.; Schulz, C. E.; Scheidt, W. R. Structural and Electronic Characterization of Nitrosyl(Octaethylporphinato)iron(III) Perchlorate Derivatives. *Inorg. Chem.* **2000**, *39*, 5102−5110.

(19) Scheidt, W. R.; Lee, Y. J.; Hatano, K. Preparation and structural characterization of nitrosyl complexes of ferric porphyrinates. Molecular structure of aquonitrosyl(meso-tetraphenylporphinato)iron-(III) perchlorate and nitrosyl(octaethylporphinato)iron(III) perchlorate. *J. Am. Chem. Soc.* **1984**, *106*, 3191−3198.

(20) Yi, G.-B.; Khan, M. A.; Richter-Addo, G. B. Activation of Thionitrites and Isoamyl Nitrite by Group 8 Metalloporphyrins and the Subsequent Generation of Nitrosyl Thiolates and Alkoxides of Ruthenium and Osmium Porphyrins. *Inorg. Chem.* **1997**, *36*, 3876−3885.

(21) Addison, A. W.; Stephanos, J. J. Nitrosyliron(III) hemoglobin: autoreduction and spectroscopy. *Biochemistry* **1986**, *25*, 4104−4113.

(22) Hoshino, M.; Maeda, M.; Konishi, R.; Seki, H.; Ford, P. C. Studies on the Reaction Mechanism for Reductive Nitrosylation of Ferrihemoproteins in Buffer Solutions. *J. Am. Chem. Soc.* **1996**, *118*, 5702−5707.

(23) Roncaroli, F.; Videla, M.; Slep, L. D.; Olabe, J. A. New features in the redox coordination chemistry of metal nitrosyls {M−NO$^+$; M−NO; M−NO$^-$(HNO)}. *Coord. Chem. Rev.* **2007**, *251*, 1903−1930.

(24) Li, J.; Peng, Q.; Oliver, A. G.; Alp, E. E.; Hu, M. Y.; Zhao, J.; Sage, J. T.; Scheidt, W. R. Comprehensive Fe−Ligand Vibration Identification in {FeNO}^{6} Hemes. *J. Am. Chem. Soc.* **2014**, *136*, 18100−18110.

(25) Ellison, M. K.; Schulz, C. E.; Scheidt, W. R. Syntheses, Characterization, and Structural Studies of Several (Nitro)(nitrosyl)-iron(III) Porphyrinates: [Fe(Porph)(NO_2)(NO)]. *Inorg. Chem.* **1999**, *38*, 100−108.

(26) Abucayon, E. G.; Khade, R. L.; Powell, D. R.; Zhang, Y.; Richter-Addo, G. B. Hydride Attack on a Coordinated Ferric Nitrosyl: Experimental and DFT Evidence for the Formation of a Heme Model−HNO Derivative. *J. Am. Chem. Soc.* **2016**, *138*, 104−107.

(27) Xu, N.; Powell, D. R.; Richter-Addo, G. B. Nitrosylation in a Crystal: Remarkable Movements of Iron Porphyrins Upon Binding of Nitric Oxide. *Angew. Chem., Int. Ed.* **2011**, *50*, 9694−9696.

(28) Xu, N.; Goodrich, L. E.; Lehnert, N.; Powell, D. R.; Richter-Addo, G. B. Preparation of the Elusive [(por)Fe(NO)(O-ligand)] Complex by Diffusion of Nitric Oxide into a Crystal of the Precursor. *Angew. Chem., Int. Ed.* **2013**, *52*, 3896−3900.

(29) Das, P. K.; Samanta, S.; McQuarters, A. B.; Lehnert, N.; Dey, A. Valence tautomerism in synthetic models of cytochrome P450. *Proc. Natl. Acad. Sci. U. S. A.* **2016**, *113*, 6611−6616.

(30) Goodrich, L. E.; Roy, S.; Alp, E. E.; Zhao, J.; Hu, M. Y.; Lehnert, N. Electronic Structure and Biologically Relevant Reactivity of Low-Spin {FeNO}^{8} Porphyrin Model Complexes: New Insight from a Bis-Picket Fence Porphyrin. *Inorg. Chem.* **2013**, *52*, 7766−7780.

(31) Praneeth, V. K. K.; Näther, C.; Peters, G.; Lehnert, N. Spectroscopic Properties and Electronic Structure of Five- and Six-

DOI: 10.1021/acs.inorgchem.7b01493
Inorg. Chem. XXXX, XXX, XXX−XXX

Coordinate Iron(II) Porphyrin NO Complexes: Effect of the Axial N-Donor Ligand. *Inorg. Chem.* **2006**, *45*, 2795−2811.
(32) Berto, T. C.; Praneeth, V. K. K.; Goodrich, L. E.; Lehnert, N. Iron-Porphyrin NO Complexes with Covalently Attached N-Donor Ligands: Formation of a Stable Six-Coordinate Species in Solution. *J. Am. Chem. Soc.* **2009**, *131*, 17116−17126.
(33) Samanta, S.; Das, P. K.; Chatterjee, S.; Sengupta, K.; Mondal, B.; Dey, A. O_2 Reduction Reaction by Biologically Relevant Anionic Ligand Bound Iron Porphyrin Complexes. *Inorg. Chem.* **2013**, *52*, 12963−12971.
(34) Chatterjee, S.; Sengupta, K.; Samanta, S.; Das, P. K.; Dey, A. Electrocatalytic O_2 Reduction Reaction by Synthetic Analogues of Cytochrome P450 and Myoglobin: In-Situ Resonance Raman and Dynamic Electrochemistry Investigations. *Inorg. Chem.* **2013**, *52*, 9897−9907.
(35) Das, P. K.; Chatterjee, S.; Samanta, S.; Dey, A. EPR, Resonance Raman, and DFT Calculations on Thiolate- and Imidazole-Bound Iron(III) Porphyrin Complexes: Role of the Axial Ligand in Tuning the Electronic Structure. *Inorg. Chem.* **2012**, *51*, 10704−10714.
(36) Chatterjee, S.; Sengupta, K.; Hematian, S.; Karlin, K. D.; Dey, A. Electrocatalytic O_2-Reduction by Synthetic Cytochrome c Oxidase Mimics: Identification of a "Bridging Peroxo" Intermediate Involved in Facile $4e^-/4H^+$ O_2-Reduction. *J. Am. Chem. Soc.* **2015**, *137*, 12897−12905.
(37) Collman, J. P.; Devaraj, N. K.; Decréau, R. A.; Yang, Y.; Yan, Y.-L.; Ebina, W.; Eberspacher, T. A.; Chidsey, C. E. D. A Cytochrome c Oxidase Model Catalyzes Oxygen to Water Reduction Under Rate-Limiting Electron Flux. *Science* **2007**, *315*, 1565−1568.
(38) Boulatov, R.; Collman, J. P.; Shiryaeva, I. M.; Sunderland, C. J. Functional Analogues of the Dioxygen Reduction Site in Cytochrome Oxidase: Mechanistic Aspects and Possible Effects of Cu_B. *J. Am. Chem. Soc.* **2002**, *124*, 11923−11935.
(39) Collman, J. P.; Fu, L.; Herrmann, P. C.; Zhang, X. A Functional Model Related to Cytochrome c Oxidase and Its Electrocatalytic Four-Electron Reduction of O_2. *Science* **1997**, *275*, 949.
(40) Garcia-Bosch, I.; Adam, S. M.; Schaefer, A. W.; Sharma, S. K.; Peterson, R. L.; Solomon, E. I.; Karlin, K. D. A "Naked" Fe^{III}-(O_2^{2-})-Cu^{II} Species Allows for Structural and Spectroscopic Tuning of Low-Spin Heme-Peroxo-Cu Complexes. *J. Am. Chem. Soc.* **2015**, *137*, 1032−1035.
(41) Wayland, B. B.; Olson, L. W. Spectroscopic studies and bonding model for nitric oxide complexes of iron porphyrins. *J. Am. Chem. Soc.* **1974**, *96*, 6037−6041.
(42) Adler, A. D.; Longo, F. R.; Kampas, F.; Kim, J. On the preparation of metalloporphyrins. *J. Inorg. Nucl. Chem.* **1970**, *32*, 2443−2445.
(43) McQuarters, A. B.; Goodrich, L. E.; Goodrich, C. M.; Lehnert, N. Disproportionation of O-Benzylhydroxylamine Catalyzed by a Ferric Bis-Picket Fence Porphyrin Complex. *Z. Anorg. Allg. Chem.* **2013**, *639*, 1520−1526.
(44) Boduszek, B.; Shine, H. J. Preparation of solid thianthrene cation radical tetrafluoroborate. *J. Org. Chem.* **1988**, *53*, 5142−5143.
(45) Paulat, F.; Berto, T. C.; DeBeer George, S.; Goodrich, L.; Praneeth, V. K. K.; Sulok, C. D.; Lehnert, N. Vibrational Assignments of Six-Coordinate Ferrous Heme Nitrosyls: New Insight from Nuclear Resonance Vibrational Spectroscopy. *Inorg. Chem.* **2008**, *47*, 11449−11451.
(46) Sage, J. T.; Paxson, C.; Wyllie, G. R. A.; Sturhahn, W.; Durbin, S. M.; Champion, P. M.; Alp, E. E.; Scheidt, W. R. Nuclear resonance vibrational spectroscopy of a protein active-site mimic. *J. Phys.: Condens. Matter* **2001**, *13*, 7707.
(47) Sturhahn, W. CONUSS and PHOENIX: Evaluation of nuclear resonant scattering data. *Hyperfine Interact.* **2000**, *125*, 149−172.
(48) *CrystalClear Expert*, 2.0 r12; Rigaku Americas Corporation: The Woodlands, TX, 2011.
(49) Sheldrick, G. M. *SHELXTL*, v. 2008/4 ed.; Bruker Analytical X-ray: Madison, WI, 2008.
(50) *CrysAlisPro*, 1.171.38.41; Rigaku Americas Corporation: The Woodlands, TX, 2015.
(51) Fernandez-Galan, R.; Manzano, B. R.; Otero, A.; Lanfranchi, M.; Pellinghelli, M. A. 19F and 31P NMR evidence for silver hexafluorophosphate hydrolysis in solution. New palladium difluorophosphate complexes and x-ray structure determination of $[Pd(\varepsilon\text{-}3\text{-}2\text{-}Me\text{-}C_3H_4)(PO_2F_2)(PCy_3)]$. *Inorg. Chem.* **1994**, *33*, 2309−2312.
(52) White, C.; Thompson, S. J.; Maitlis, P. M. Pentamethylcyclopentadienyl-rhodium and-iridium complexes XIV. The solvolysis of coordinated acetone solvent species to tris(μ-difluorophosphato)bis-[η5-pentamethylcyclopentadienylrhodium(III)] hexafluorophosphate, to the η5-(2,4-dimethyl-1-oxapenta-1,3-dienyl)-(pentamethylcyclopentadienyl)iridium cation, or to the η5-(2-hydroxy-4-methylpentadienyl)(η5-pentamethylcyclopentadienyl)-iridium cation. *J. Organomet. Chem.* **1977**, *134*, 319−325.
(53) Mu, X. H.; Kadish, K. M. In situ FTIR and UV-visible spectroelectrochemical studies of iron nitrosyl porphyrins in non-aqueous media. *Inorg. Chem.* **1988**, *27*, 4720−4725.
(54) Ozawa, S.; Sakamoto, E.; Ichikawa, T.; Watanabe, Y.; Morishima, I. Model Studies of Nitrosyl Intermediates in the Catalytic Cycle of Dissimilatory Nitrite Reductases. *Inorg. Chem.* **1995**, *34*, 6362−6370.
(55) Connelly, N. G.; Geiger, W. E. Chemical Redox Agents for Organometallic Chemistry. *Chem. Rev.* **1996**, *96*, 877−910.
(56) Quinn, R.; Nappa, M.; Valentine, J. S. New five- and six-coordinate imidazole and imidazolate complexes of ferric tetraphenylporphyrin. *J. Am. Chem. Soc.* **1982**, *104*, 2588−2595.
(57) Laverman, L. E.; Ford, P. C. Mechanistic Studies of Nitric Oxide Reactions with Water Soluble Iron(II), Cobalt(II), and Iron(III) Porphyrin Complexes in Aqueous Solutions: Implications for Biological Activity. *J. Am. Chem. Soc.* **2001**, *123*, 11614−11622.
(58) Safo, M. K.; Walker, F. A.; Raitsimring, A. M.; Walters, W. P.; Dolata, D. P.; Debrunner, P. G.; Scheidt, W. R. Axial Ligand Orientation in Iron(III) Porphyrinates: Effect of Axial π-Acceptors. Characterization of the Low-Spin Complex $[Fe(TPP)(4\text{-}CNPy)_2]$-$ClO_4$. *J. Am. Chem. Soc.* **1994**, *116*, 7760−7770.
(59) Lim, M. D.; Lorkovic, I. M.; Ford, P. C. NO and NO_x interactions with group 8 metalloporphyrins. *J. Inorg. Biochem.* **2005**, *99*, 151−165.
(60) Grande, L. M.; Noll, B. C.; Oliver, A. G.; Scheidt, W. R. Dynamics of NO Motion in Solid-State [Co(tetraphenylporphinato)-(NO)]. *Inorg. Chem.* **2010**, *49*, 6552−6557.
(61) Praneeth, V. K. K.; Neese, F.; Lehnert, N. Spin Density Distribution in Five- and Six-Coordinate Iron(II)−Porphyrin NO Complexes Evidenced by Magnetic Circular Dichroism Spectroscopy. *Inorg. Chem.* **2005**, *44*, 2570−2572.
(62) Vogel, K. M.; Kozlowski, P. M.; Zgierski, M. Z.; Spiro, T. G. Determinants of the FeXO (X = C, N, O) Vibrational Frequencies in Heme Adducts from Experiment and Density Functional Theory. *J. Am. Chem. Soc.* **1999**, *121*, 9915−9921.
(63) Soldatova, A. V.; Ibrahim, M.; Olson, J. S.; Czernuszewicz, R. S.; Spiro, T. G. New Light on NO Bonding in Fe(III) Heme Proteins from Resonance Raman Spectroscopy and DFT Modeling. *J. Am. Chem. Soc.* **2010**, *132*, 4614−4625.
(64) Linder, D. P.; Rodgers, K. R.; Banister, J.; Wyllie, G. R. A.; Ellison, M. K.; Scheidt, W. R. Five-Coordinate $Fe^{III}NO$ and $Fe^{II}CO$ Porphyrinates: Where Are the Electrons and Why Does It Matter? *J. Am. Chem. Soc.* **2004**, *126*, 14136−14148.
(65) Benko, B.; Yu, N. T. Resonance Raman studies of nitric oxide binding to ferric and ferrous hemoproteins: detection of Fe(III)–NO stretching, Fe(III)–N–O bending, and Fe(II)–N–O bending vibrations. *Proc. Natl. Acad. Sci. U. S. A.* **1983**, *80*, 7042−7046.
(66) Maes, E. M.; Walker, F. A.; Montfort, W. R.; Czernuszewicz, R. S. Resonance Raman Spectroscopic Study of Nitrophorin 1, a Nitric Oxide-Binding Heme Protein from Rhodnius prolixus, and Its Nitrosyl and Cyano Adducts. *J. Am. Chem. Soc.* **2001**, *123*, 11664−11672.
(67) Goodrich, L. E.; Paulat, F.; Praneeth, V. K. K.; Lehnert, N. Electronic Structure of Heme-Nitrosyls and Its Significance for Nitric Oxide Reactivity, Sensing, Transport, and Toxicity in Biological Systems. *Inorg. Chem.* **2010**, *49*, 6293−6316.

DOI: 10.1021/acs.inorgchem.7b01493
Inorg. Chem. XXXX, XXX, XXX−XXX

(68) Xu, N.; Powell, D. R.; Cheng, L.; Richter-Addo, G. B. The first structurally characterized nitrosyl heme thiolate model complex. *Chem. Commun.* **2006**, 2030−2032.
(69) Paulat, F.; Lehnert, N. Electronic Structure of Ferric Heme Nitrosyl Complexes with Thiolate Coordination. *Inorg. Chem.* **2007**, *46*, 1547−1549.
(70) Hu, S.; Kincaid, J. R. Resonance Raman characterization of nitric oxide adducts of cytochrome P450cam: the effect of substrate structure on the iron-ligand vibrations. *J. Am. Chem. Soc.* **1991**, *113*, 2843−2850.
(71) Obayashi, E.; Tsukamoto, K.; Adachi, S.-i.; Takahashi, S.; Nomura, M.; Iizuka, T.; Shoun, H.; Shiro, Y. Unique Binding of Nitric Oxide to Ferric Nitric Oxide Reductase from Fusarium oxysporum Elucidated with Infrared, Resonance Raman, and X-ray Absorption Spectroscopies. *J. Am. Chem. Soc.* **1997**, *119*, 7807−7816.
(72) Hu, S.; Kincaid, J. R. Resonance Raman spectra of the nitric oxide adducts of ferrous cytochrome P450cam in the presence of various substrates. *J. Am. Chem. Soc.* **1991**, *113*, 9760−9766.
(73) Hu, S.; Kincaid, J. R. Heme active-site structural characterization of chloroperoxidase by resonance Raman spectroscopy. *J. Biol. Chem.* **1993**, *268*, 6189.
(74) Miller, L. M.; Pedraza, A. J.; Chance, M. R. Identification of conformational substates involved in nitric oxide binding to ferric and ferrous myoglobin through difference fourier transform infrared spectroscopy (FTIR). *Biochemistry* **1997**, *36*, 12199−12207.
(75) Tomita, T.; Haruta, N.; Aki, M.; Kitagawa, T.; Ikeda-Saito, M. UV Resonance Raman Detection of a Ligand Vibration on Ferric Nitrosyl Heme Proteins. *J. Am. Chem. Soc.* **2001**, *123*, 2666−2667.
(76) Wang, Y.; Averill, B. A. Direct Observation by FTIR Spectroscopy of the Ferrous Heme−NO+ Intermediate in Reduction of Nitrite by a Dissimilatory Heme cd1 Nitrite Reductase. *J. Am. Chem. Soc.* **1996**, *118*, 3972−3973.
(77) Sampath, V.; Zhao, X.; Caughey, W. S. Characterization of interactions of nitric oxide with human hemoglobin A by infrared spectroscopy original. *Biochem. Biophys. Res. Commun.* **1994**, *198*, 281−287.
(78) Ding, X. D.; Weichsel, A.; Andersen, J. F.; Shokhireva, T. K.; Balfour, C.; Pierik, A. J.; Averill, B. A.; Montfort, W. R.; Walker, F. A. Nitric Oxide Binding to the Ferri- and Ferroheme States of Nitrophorin 1, a Reversible NO-Binding Heme Protein from the Saliva of the Blood-Sucking Insect, Rhodnius prolixus. *J. Am. Chem. Soc.* **1999**, *121*, 128−138.

DOI: 10.1021/acs.inorgchem.7b01493
Inorg. Chem. XXXX, XXX, XXX−XXX